



저작자표시-비영리-변경금지 2.0 대한민국

이용자는 아래의 조건을 따르는 경우에 한하여 자유롭게

- 이 저작물을 복제, 배포, 전송, 전시, 공연 및 방송할 수 있습니다.

다음과 같은 조건을 따라야 합니다:



저작자표시. 귀하는 원저작자를 표시하여야 합니다.



비영리. 귀하는 이 저작물을 영리 목적으로 이용할 수 없습니다.



변경금지. 귀하는 이 저작물을 개작, 변형 또는 가공할 수 없습니다.

- 귀하는, 이 저작물의 재이용이나 배포의 경우, 이 저작물에 적용된 이용허락조건을 명확하게 나타내어야 합니다.
- 저작권자로부터 별도의 허가를 받으면 이러한 조건들은 적용되지 않습니다.

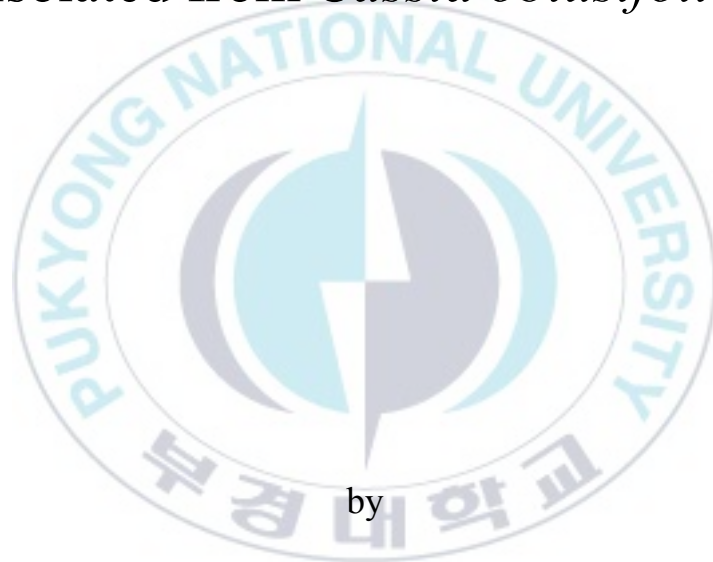
저작권법에 따른 이용자의 권리는 위의 내용에 의하여 영향을 받지 않습니다.

이것은 [이용허락규약\(Legal Code\)](#)을 이해하기 쉽게 요약한 것입니다.

[Disclaimer](#)

Thesis for the Degree of Master of Science

*In vitro* structure related inhibition of enzyme  
system in cholinesterases and BACE1 by naturally  
occurring naphthopyrone and its glycosides  
isolated from *Cassia obtusifolia*



by

Srijan Shrestha

Department of Food and Life Science

The Graduate School

Pukyong National University

February 23, 2018

*In vitro* structure related inhibition of enzyme system in  
cholinesterases and BACE1 by naturally occurring  
naphthopyrone and its glycosides isolated from *Cassia  
obtusifolia*

(알츠하이머 질환 관련 효소계에 대한 결명자로부터  
분리된 naphthopyrone과 그 배당체 구조와 억제활성  
상관관계)

Advisor: Prof. Jae Sue Choi

by

Srijan Shrestha

A thesis submitted in partial fulfillment of the requirements for the degree of

Master of Science

in Department of Food and Life Science, The Graduate School

Pukyong National University

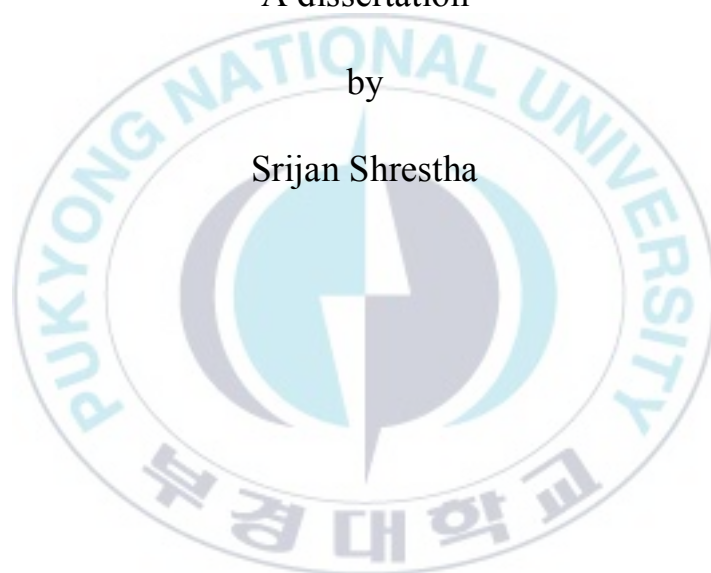
February 23, 2018

*In vitro* structure related inhibition of enzyme system in cholinesterases and  
BACE1 by naturally occurring naphthopyrone and its glycosides isolated from  
*Cassia obtusifolia*

A dissertation

by

Srijan Shrestha



Approved by:

A handwritten signature in black ink, appearing to read 'T. J. Nam', written over a horizontal line.

(Chairman) Taek Jeong Nam

A handwritten signature in black ink, appearing to read 'Hyeung Rak Kim', written over a horizontal line.

(Member) Hyeung Rak Kim

A handwritten signature in black ink, appearing to read 'Jae Sue Choi', written over a horizontal line.

(Member) Jae Sue Choi

February 23, 2018

# Contents

List of Schemes .....	iii
List of Figures .....	iv
List of Tables.....	vi
Abbreviations.....	vii
요 약 .....	ix
<b>I . Introduction</b> .....	<b>1</b>
<b>II . Materials and methods</b> .....	<b>4</b>
1. Plant materials.....	4
2. General experimental procedures.....	4
3. Chemicals and Reagents .....	4
4. Experimental methods.....	5
4-1. Extraction, fractionation and isolation.....	5
4-2. <i>In vitro</i> ChEs enzyme assay.....	15
4-3. BACE1 inhibitory assay .....	16
4-4. Enzyme kinetic analysis with BChE and BACE1.....	17
4-5. Molecular docking simulation .....	17
5. Statistical analysis.....	19
<b>III. Results</b> .....	<b>20</b>
1. Inhibitory activities of rubrofusarin and its derivatives against AChE, BChE and BACE1.....	20
2. Enzyme kinetic analysis of active compounds with AChE and BACE1.....	21

3. Molecular docking simulation in AChE inhibition .....	24
4. Molecular docking simulation in BACE1 inhibition .....	29
<b>IV. Discussion</b> .....	<b>33</b>
<b>V. Conclusion</b> .....	<b>38</b>
<b>VI. References</b> .....	<b>39</b>



## List of Schemes

<b>Scheme</b>	<b>Page</b>
Scheme 1. Extraction and fractionation of seeds of <i>Cassia obtusifolia</i> .....	7
Scheme 2. Isolation of compounds from water portion of <i>Cassia obtusifolia</i> .....	8



## List of Figures

Figure	Page
Figure 1. Chemical structures of isolated compounds. ....	10
Figure 2. Dixon plots and Lineweaver-Burk plots for AChE inhibition by <b>3</b> . The results showed the effects of presence of different concentrations of the substrate (0.6 (●), 0.3 (○), and 0.1 mM (▼)) for (A) and the effect of presence of different concentrations of <b>3</b> (0 (●), 4 (○), 20 (▼), and 50 μM (Δ)) for (B). ....	23
Figure 3. Dixon plots and Lineweaver-Burk plots for BACE1 inhibition by <b>4</b> . The results showed the effects of presence of different concentrations of the substrate (252 (●), 375 (○), and 750 nM (▼)) for (A) and the effect of presence of different concentration of (B) <b>4</b> (0 (●), 5 (○), 10 (▼), and 25 μM (Δ)). ....	23
Figure 4. Inhibition mode of <b>3</b> (A) for the AChE active site with tacrine ( <i>red stick</i> ) (A). 2D ligand interaction diagram of AChE catalytic inhibition by <b>3</b> (B). Dashed lines indicate H-bonds. Carbons are in black, nitrogens in blue, and oxygens in red. The figure was generated using PyMOL and Ligplot. ....	26
Figure 5. Inhibition mode of <b>1</b> (A), <b>2</b> (B), and <b>3</b> (C) for the AChE allosteric site with donepezil ( <i>blue stick</i> ) (A). 2D ligand interaction diagram of AChE allosteric inhibition by <b>1</b> (D), <b>2</b> (E), and <b>3</b> (F). Dashed lines indicate H-bonds. Carbons are in black, nitrogen in blue, and oxygen in red. The figure was generated using PyMOL and Ligplot. ....	27
Figure 6. Inhibition mode of <b>4</b> (A) and <b>2</b> (B) for the BACE1 catalytic site with QUD ( <i>red</i>	

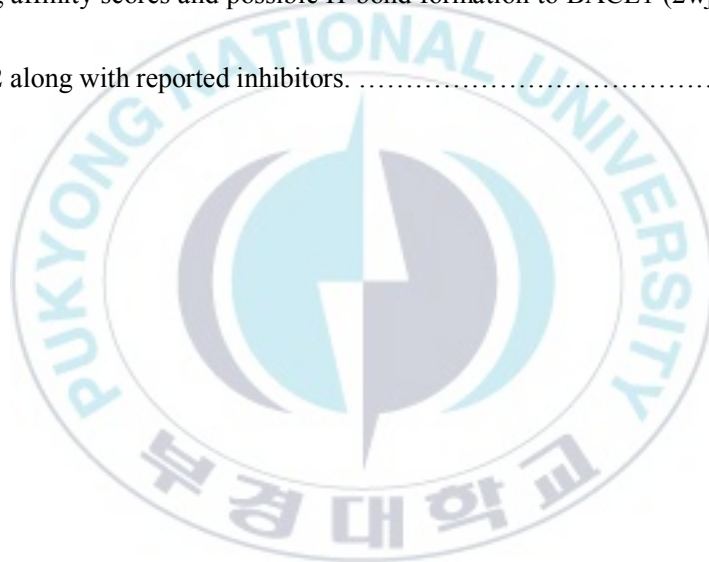
*stick*) (A). 2D ligand interaction diagrams of BACE1 catalytic inhibition by **4** (C) and **2** (D). Dashed lines indicate H-bonds. Carbons are in black, nitrogens in blue, and oxygen in red. The figure was generated using PyMOL and Ligplot. ....30

Figure 7. Inhibition mode of **4** for the BACE1 allosteric site with PMF (*blue stick*) (A). 2D ligand interaction diagram of BACE1 allosteric (B) inhibition by **4**. Dashed lines indicate H-bonds. Carbons are in black, nitrogens in blue, and oxygens in red. The figure was generated using PyMOL and Ligplot. .... 31



## List of Tables

Table	Page
Table 1. Cholinesterase and BACE1 inhibitory activity of compounds isolated from <i>Cassia obtusifolia</i> . .....	22
Table 2. Docking affinity scores and possible H-bond formation to AChE (1acj) active sites by <b>1</b> , <b>2</b> , and <b>3</b> along with reported inhibitors. ....	28
Table 3. Docking affinity scores and possible H-bond formation to BACE1 (2wjo) active sites by <b>4</b> and <b>2</b> along with reported inhibitors. ....	32



## Abbreviations

A $\beta$	: Amyloid $\beta$
ACh	: Acetylcholine
AChE	: Acetylcholinesterase
AD	: Alzheimer's disease
ADT	: AutoDock Tool
APP	: Amyloid precursor protein
ATCh	: Acetylthiocholine iodide
BACE1	: $\beta$ -site amyloid precursor protein cleaving enzyme 1
BChE	: Butyrylcholinesterase
BTCh	: Butyrylthiocholine chloride
BuOH	: <i>n</i> -butanol
<i>C. obtusifolia</i>	: <i>Cassia obtusifolia</i>
CH <sub>2</sub> Cl <sub>2</sub>	: Dichloromethane
ChEs	: Cholinesterases
DMSO	: Dimethyl sulfoxide
DTNB	: 5,5'-dithiobis-(2-nitrobenzoic acid)
EtOAc	: Ethyl acetate
GA	: Genetic algorithm
IC <sub>50</sub>	: Half inhibitory concentration
<i>K<sub>i</sub></i>	: Inhibition constant
MeOH	: Methanol
NCBI	: PubChem Compound
QUD	: 2-amino-3-((1 <i>R</i> )-1-cyclohexyl-2-[(cyclohexylcarbonyl)amino]ethyl)-6-phenoxyquinazolin-3-ium
SARs	: Structure-activity relationships
Si	: Silica
TLC	: Thin layer chromatography

THA : Tacrine  
PMF : 3,5,7,3',4'-pentamethoxyflavone



알츠하이머 질환 관련 효소계에 대한 결명자로부터 분리된 naphthopyrone과 그 배당체

## 구조와 억제활성 상관관계

Srijan Shrestha

부경대학교 대학원 식품생명과학과

### 요 약

결명자는 고대부터 시력 향상, 염증 질환 개선, 간해독제 그리고 배뇨작용을 촉진시키는데 사용되어 왔다. 결명자의 항염증, 항산화, 신경보호효과와 항균효과가 보고된바 있다. 최근, 결명자의 폭넓고 다양한 생리활성 화합물들의 존재 때문에 알츠하이머 질환의 치료를 위한 천연 약물의 원천으로 대두되고 있다. 이번 연구에서, 결명자로부터 다양한 화합물들이 분리되었고 여러 화합물들 중 naphthopyrone 유도체들을 알츠하이머 질환과 관련이 있는 아세틸콜린에스테라아제 (AChE), 부티릴콜린에스테라아제 (BChE) 그리고 BACE1의 저해에 대한 glycosylation의 영향과 구조-활성 상관관계를 조사하기 위해서 실험에 사용하였다. 결명자로부터 유래된 6개의 화합물 (rubrofusarin (1), rubrofusarin 6-*O*- $\beta$ -D-glucopyranoside (2), rubrofusarin 6-*O*- $\beta$ -D-gentiobioside (3), nor-rubrofusarin 6-*O*- $\beta$ -D-glucoside (4), isorubrofusarin 10-*O*- $\beta$ -D-gentiobioside (5) 그리고 rubrofusarin 6-*O*- $\beta$ -D-triglucoside (6)) 모두 AChE와 BACE1에 대하여 저해효과를 나타내었다. 특히, 3번과 4번 화합물이 각각 AChE와 BACE1에 가장 높은 저해율을 보였다. 반면에, 2, 5 그리고 6번 화합물은 두 효소의 저해에 보통의 효과를 보였다. 구조-활성 상관관계 결과는 AChE 저해에는 rubrofusarin에 gentiobiosyl 작용기가 중요하고 AChE/BACE1 저해에는 naphthalene 고리의 C-8 위치에 -OH 또는 -OCH<sub>3</sub>작용기의 존재와  $\beta$  또는  $\gamma$  위치의 pyrone 고리 배열이 중요하다는 것을 강조하였다. 효소반응속도 연구와 도킹 결과는 3번 화합물이 AChE에 음의 결합 에너지와 높은 친화력을 가지는 혼합형 저해제임을 보여주었다. 소수성 상호작용과 수소결합은 효소-저해제 상호작용의 강한 결합력을 나타낸다. 따라서, 이번 연구의 결과는 결명자와 그 구성성분이 알츠하이머 질환에 대하여 치료적 효과가 있고 활성 화합물의 구조-활성 상관관계가 더 연구되어야 할 것을 제시한다.

# . Introduction

Structure-activity relationships (SARs) link molecular structures with properties, effects, or biological activities (McKinney et al., 2000). SARs studies are fundamental to many phases of drug discovery from primary screening to lead development. These studies start with the identification of a collection of molecules of interest and then following this with studies that establish relationships between molecular structures and observed activities to identify structural features that enhance properties or functionalities of interest (Guha et al., 2013). Due to time and cost restraints, it is not possible to test all compounds of interest thoroughly, and thus, SAR studies help predict biological responses and determine the direction of future developments in a cost and time effective manner (Schultz et al., 1983). The biological activities of a new chemical species can often be predicted from its molecular structure using other similar compounds database. Accordingly, SAR studies are powerful tool for understanding functional implications of unknowns when molecular similarities are evident.

Fukuda et al. (2009) demonstrated that hydroxyl groups at C-1 or C-4 but not in the C-3 position of anthraquinone structures are crucial for the dominating effect of DNA-binding activity of the aryl hydrocarbon receptor induced by 2,3,7,8-tetrachlorodibenzo-*p*-dioxin. Luo et al. (2014) reported the hydroxyl group of new series of aryl naphthalene lignans significantly increases antitumor activity while a methoxy group decreases its activity, and others have reported the location and types of sugar moieties on aglycone skeletons greatly influence biological activity. Lim et al. (2006) demonstrated the influence of sugar derivatives of kaempferol, isorhamnetin and quercetin in the intensity of their aldose reductase inhibitory activity, and Choudhury et al. (1999) suggested the influence of deglycosylation of flavonoids in the expression of their bioactivity. Furthermore, the antioxidant activity of flavonol glycosides in tea were found to decline as the number of glycosidic moieties increased (Ratty et al., 1988).

Alzheimer's disease (AD) is the most predominant neurodegenerative disorder found in the elderly. It has been reported, more than 46.8 million people suffer from

AD, and that associated annual medical costs exceed \$818 billion. In the same report, it was estimated that more than 131.5 million individuals will have AD in the year 2050 (Prince et al., 2015). Life expectancy after clinical symptom onset is around 8.5 years (Chertkow et al., 2008). But until now, there is no effective treatment that targets the underlying molecular causes of disease. Although the absolute pathophysiological mechanism of the disease is not clear, two hypothesis have been proposed that are, the "cholinergic hypothesis" and the "amyloid hypothesis". According to the cholinergic hypothesis, an insufficiency of cholinergic functions in the brain results in the memory impairments. The use of acetylcholinesterase (AChE) and butyrylcholinesterase (BChE) inhibitors (enzymes responsible for metabolic hydrolysis of acetylcholine) which increase the availability of acetylcholine at cholinergic synapses, offer a promising therapeutic strategy for activation of central cholinergic function (Francis et al., 1999). On the other hand, the amyloid hypothesis states that amyloid- $\beta$  peptide ( $A\beta$ ) accumulation in the brain is responsible for the pathogenesis of AD. Amyloid plaques, which is primarily composed of  $A\beta$ , gradually form in the brains of AD patients, and mutations in amyloid precursor protein, presenilin 1 and 2 cause early-onset familial AD by directly increasing toxic, plague-promoting  $A\beta$  production. BACE1 displays all the functional properties of  $\beta$ -secretase and is a key enzyme in the  $A\beta$  formation, and thus, BACE1 is an appropriate target site for drug (Vassar et al., 2004).

Cassia semen (sicklepod) is the seed of an annual plant *Cassia obtusifolia* L. (Leguminosae), which is grown widely in Korea and China. Traditionally, Cassia seed has been used to treat dizziness, headache, improve vision and as hepatoprotective agents (Ju et al., 2010) and has been reported to have antioxidant effects (Yen et al., 2010), neuroprotection effects in Parkinson's disease models (Ju et al., 2010), to attenuate scopolamine induced memory impairment or transient cerebral hypoperfusion in mice (Kim et al., 2007), to ameliorated amyloid  $\beta$ -induced synaptic dysfunction through anti-inflammatory and Akt/GSK-3 $\beta$  pathways (Yi et al., 2016), to attenuate secondary calcium dysregulation and to have neuroprotective effect against mitochondrial toxin (which has been implicated in pathogenesis of AD) in mouse

primary hippocampal cultures (Drever et al., 2008), to have antimicrobial activity (Kitanaka et al., 1986) and to inhibit protein glycation and aldose reductase activity in vitro (Jang et al., 2007).

Rubrofusarin and its derivatives isolated from *C. obtusifolia* have been reported to have anti-cancer effects (Megawati et al., 2017), hepatoprotective effects (Wong et al., 1989), advanced glycation end products inhibitory (Lee et al., 2006), 1,1-diphenyl-2-picrylhydrazyl (DPPH) radical scavenging (Choi et al., 1994), antioxidant (Park et al., 2004), anti-AD (Jung et al., 2016a), anti-diabetes (Jung et al., 2016b), anti-estrogenic (El-Halawany et al., 2007), and antimycobacterial (Graham et al., 2004) activities. Many investigations have been performed on the SARs of flavonoids but nothing has yet been published on the SARs of naphthopyrone and its derivatives (rubrofusarin being categorized in the naphthopyrone class). In previous investigation, the inhibitory activities of major chemical constituents isolated from *C. obtusifolia* against  $\beta$ -secretase and cholinesterase were reported (Jung et al., 2016a). Among the various fractions in methanolic extract of *C. obtusifolia*, *n*-butanol (BuOH) fraction exhibited most potent inhibitory activities against  $\beta$ -secretase and cholinesterase. Different compounds were isolated from this fraction and among them, toralactone gentiobioside showed moderate activity whereas nor-rubrofusarin 6-*O*- $\beta$ -D-glucoside exhibited most potent BACE1 inhibitory activity. It is interesting to note that both compounds share structural similarity but exhibit diverse activity and there were reports regarding the presence of structural analogs in the cassia seeds (Jung et al., 2016a). Therefore, we performed further analysis to isolate structural analogs (naphthopyrones) accordingly, with the aim of investigating the SARs of naphthopyrones isolated from *C. obtusifolia*. Fourteen compounds were isolated from the water portion of *C. obtusifolia* methanolic extract. Among them, we selected structural analogs, (rubrofusarin and its derivatives) in order to investigate the influences of (i) glycosylation (ii) C-8 methoxy group (iii) pyrone ring arrangement at the naphthalene ring on their biological activities against cholinesterases and BACE1. In addition, we performed kinetic and molecular studies to determine the exact orientation of compounds in the active site of specific enzyme.

# . Materials and methods

## 1. Plant materials

Raw seeds of *Cassia obtusifolia* were purchased (Omni Herb Co.) and identified by Prof. J.-H. Lee (Dongguk University, Gyeongju). A voucher specimen (no. 20160302) was registered and deposited in the Prof. J. S. Choi laboratory (Pukyong National University, Busan). Department of Food and life Science, Pukyong National University, Busan, Republic of Korea. A voucher specimen (No. 20160115) was deposited in the laboratory of Prof. J. S. Choi.

## 2. General experimental procedures

The  $^1\text{H}$ - and  $^{13}\text{C}$ -NMR spectra were recorded in dimethyl sulfoxide (DMSO- $d_6$ ) on a JEOL JNM ECP-400 spectrometer (Tokyo, Japan) at 400/600 MHz and 100 MHz, respectively. Column chromatography was performed using Diaion HP-20, Sephadex LH-20 (20-100  $\mu\text{M}$ , Sigma, St. Louis, MO, USA), silica (Si) gel 60 (70-230 mesh, Merck, Darmstadt, Germany), LiChroprep RP-18 (40-63  $\mu\text{M}$ , Merck, Darmstadt, Germany). All TLC were performed on a precoated Merck Kiesel gel 60 F<sub>254</sub> plates (20  $\times$  20 cm, 0.25 mm) and RP-18 F<sub>254S</sub> plates (5  $\times$  10 cm, Merck, Darmstadt, Germany). The spray reagent was 50% H<sub>2</sub>SO<sub>4</sub>.

## 3. Chemicals and Reagents

Electric-eel AChE (EC 3.1.1.7), horse-serum BChE (EC 3.1.1.8), acetylthiocholine iodide (ACh), butyrylthiocholine chloride (BCh), 5,5'-dithiobis-(2-nitrobenzoic acid) (DTNB), quercetin, and berberine were purchased from Sigma Co.

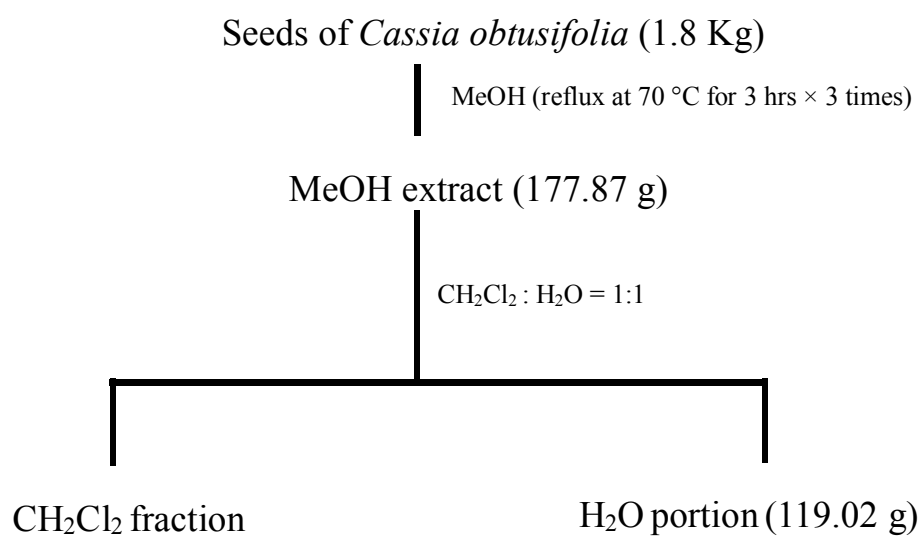
(St. Louis, MO, U.S.A.). A BACE1 fluorescence resonance energy transfer (FRET) assay kit ( $\beta$ -secretase) was purchased from Pan Vera Co. (Madison, WI, U.S.A.). All chemicals and solvents used in column chromatography and assays were of reagent grade and were purchased from commercial sources.

## 4. Experimental methods

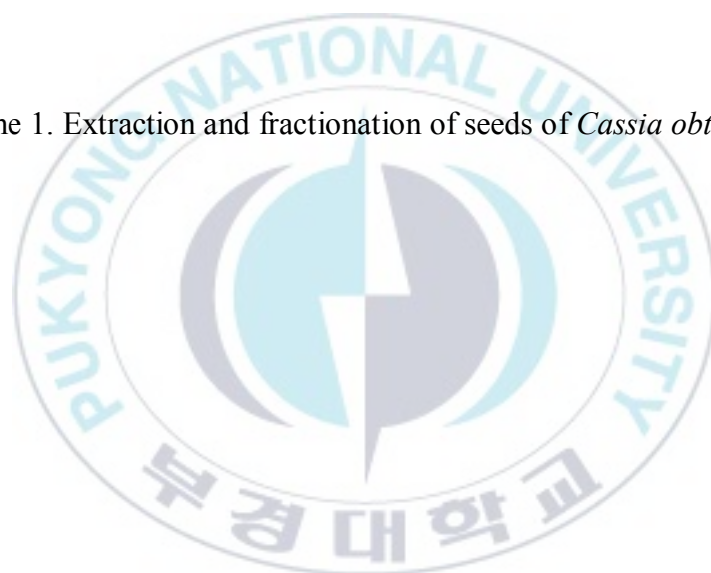
### 4-1. Extraction, fractionation and isolation

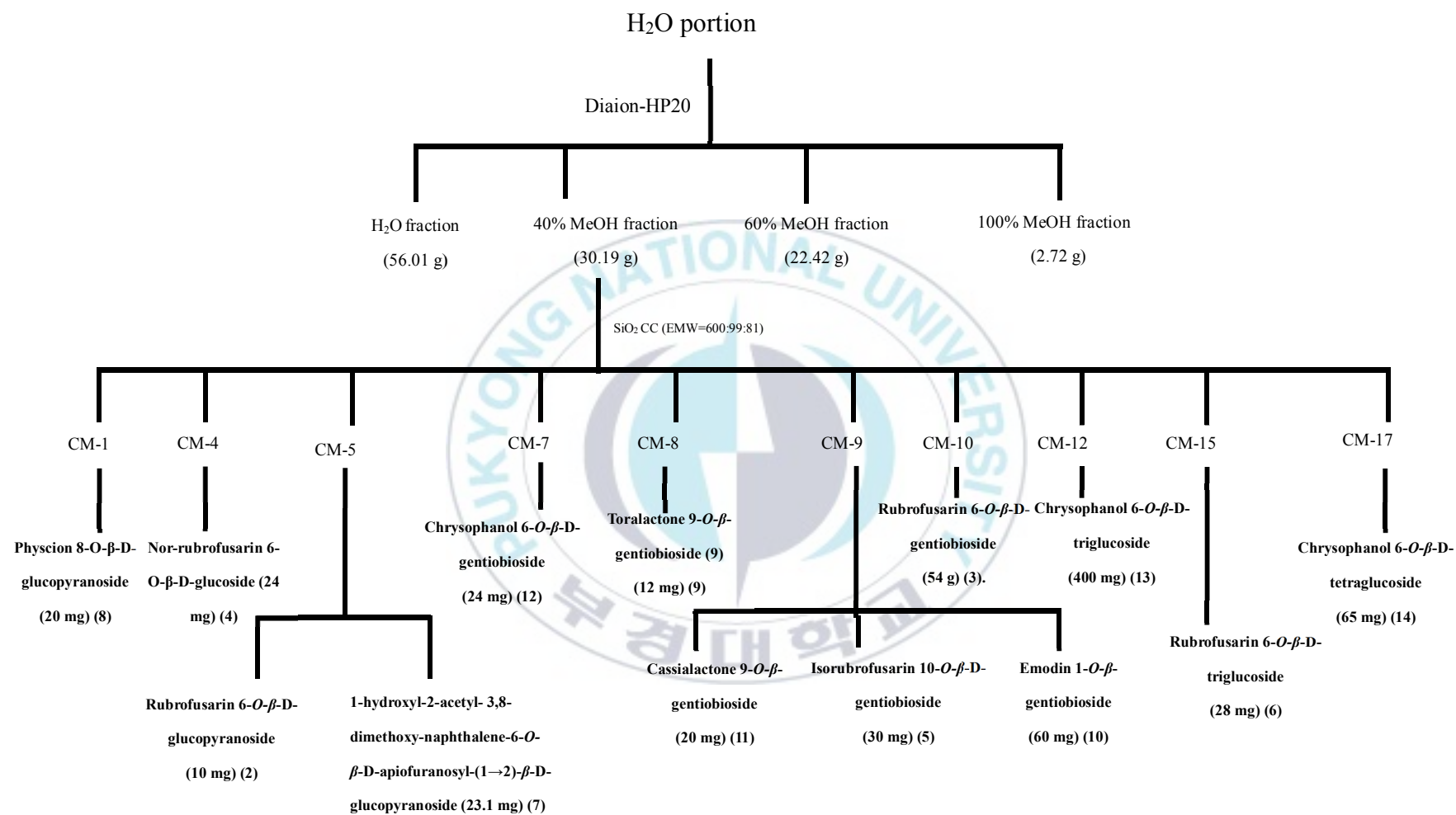
The seeds of *C. obtusifolia* (1.8 kg) were refluxed in methanol (MeOH) (3 h  $\times$  5 times). The total filtrate was then dried using evaporator under reduced pressure to produce the MeOH extract. The extract was suspended in distilled water and continuously partitioned with dichloromethane to get dichloromethane fraction and water residue. The water residue (119.02 g) was subjected to column chromatography (Diaion HP-20) and eluted with distilled water, 40% MeOH, 60% MeOH and 100% MeOH, gradually to obtain four subfractions of 56.01 g, 30.19 g, 22.42 g and 2.72 g, respectively. The 40% MeOH subfraction was subjected to Si gel chromatography and eluted with ethyl acetate: MeOH: water (EMW = 600:99:81) to yield 20 subfractions. Subfraction 1 was subjected to Si gel column chromatography using dichloromethane: MeOH: water (CMW = 7:1:0.1) to get physcion 8-*O*- $\beta$ -D-glucopyranoside (20 mg) (**8**). Subfraction 4 was subjected to Si gel chromatography using CMW (7:1:0.1) to obtain nor-rubrofusarin 6-*O*- $\beta$ -D-glucoside (12 mg) (**4**). Subfraction 5 was subjected to repeated Si gel chromatography using EMW and CMW in various ratio to get rubrofusarin 6-*O*- $\beta$ -D-glucopyranoside (10 mg) (**2**) and 1-hydroxyl-2-acetyl-3,8-dimethoxy-naphthalene-6-*O*- $\beta$ -D-apiofuranosyl-(1 $\rightarrow$ 2)- $\beta$ -D-glucopyranoside (23.1 mg) (**7**). Precipitate obtained from subfraction 7 was washed with methanol first and was subjected to Si gel CC using EMW (600:99:81) to get chrysophanol 6-*O*- $\beta$ -D-gentiobioside (24 mg) (**12**). Subfraction 8 was subjected to Si gel CC using CMW (4:1:0.1) to get toralactone 9-*O*- $\beta$ -gentiobioside (**9**) (12 mg). Subfraction 9 was

subjected to repeated chromatography using EMW and CMW in various ratio to get cassialactone 9-*O*- $\beta$ -gentiobioside (20 mg) (**11**), isorubrofusarin 10-*O*- $\beta$ -D-gentiobioside (30 mg) (**5**), and emodin 1-*O*- $\beta$ -gentiobioside (60 mg) (**10**). The precipitate obtained from subfraction 10 was chromatographed over Si gel using EMW (600:99:81) to get rubrofusarin 6-*O*- $\beta$ -D-gentiobioside (54 g) (**3**). Chrysophanol 6-*O*- $\beta$ -D-triglucoside (400 mg) (**13**) was obtained from subfraction 12 as a precipitate (purified by washing with MeOH and EtOAc). Subfraction 15 was chromatographed over Si gel using EMW (21:5:3) as solvent system to get to rubrofusarin 6-*O*- $\beta$ -D-triglucoside (28 mg) (**6**). The precipitate obtained from subfraction 17 was chromatographed over Si gel using EMW (21:5:3) as solvent system to get chrysophanol 6-*O*- $\beta$ -D-tetraglucoside (65 mg) (**14**). Subfraction 1 of 100% MeOH sub fraction was subjected to Si gel chromatography and eluted with CMW (15:1:0.1) to get rubrofusarin (35 mg) (**1**). All compounds were characterized and identified by spectroscopic methods ( $^1\text{H}$ - and  $^{13}\text{C}$ -NMR) and also matched with the previously published data (Lee et al., 2006; Messana et al., 1991; Lee et al., 1997; Na et al., 2008; Hatano et al., 1999; Wang et al., 2007; Youn et al., 2017; Zhang et al., 2011) and chrysophanol glucosides and toralactone gentiobioside were confirmed by comparing the TLC pattern by using EMW, CMW in various ratio with the standard. The structure of these compounds are shown in Fig. 1.

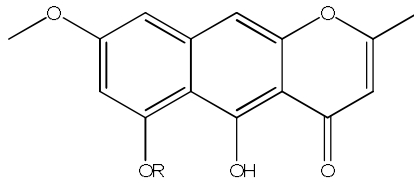


Scheme 1. Extraction and fractionation of seeds of *Cassia obtusifolia*





Scheme 2. Isolation of compounds from water portion of *Cassia obtusifolia*



R= H

**Rubrofusarin (1)**

R= glu

**Rubrofusarin 6-*O*- $\beta$ -D-glucopyranoside (2)**

R= glu (1 $\rightarrow$ 6) glu

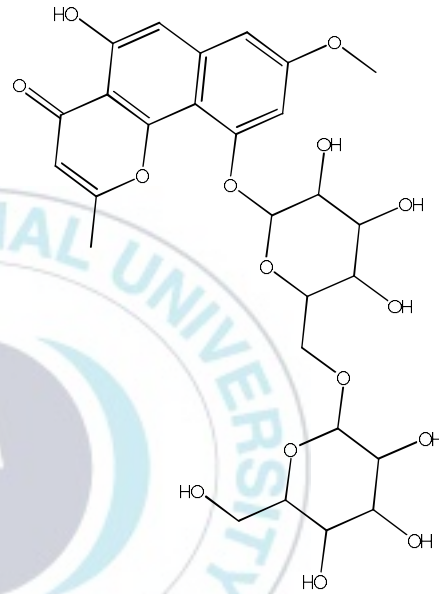
**Rubrofusarin 6-*O*- $\beta$ -D-gentiobioside (3)**

R= glu (1 $\rightarrow$ 6) glu (1 $\rightarrow$ 3) glu

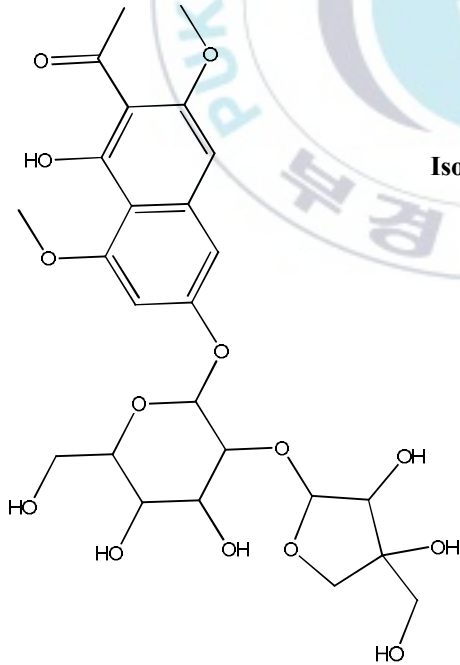
**Rubrofusarin 6-*O*- $\beta$ -D-triglucoside (6)**



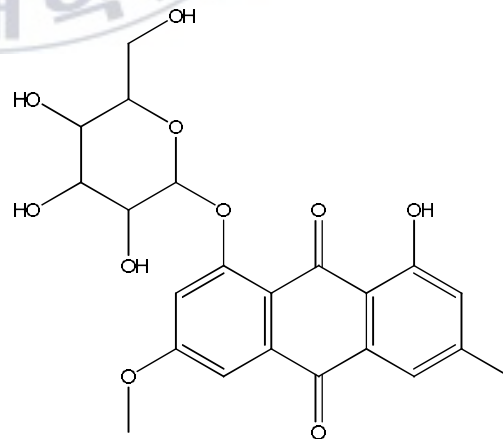
**Nor-rubrofusarin 6-*O*- $\beta$ -D-glucoside (4)**



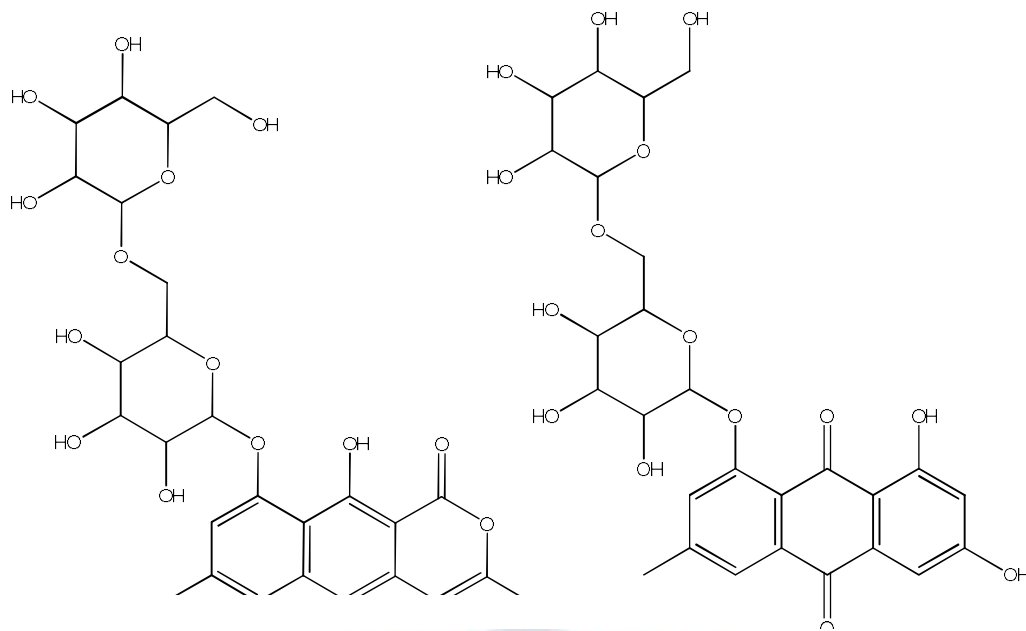
**Isorubrofusarin 10-*O*- $\beta$ -D-gentiobioside (5)**



**1-hydroxyl-2-acetyl-3,8-dimethoxynaphthalene 6-*O*- $\beta$ -D-apiofuranosyl-(1 $\rightarrow$ 2)- $\beta$ -D-gluconvranoside (7)**

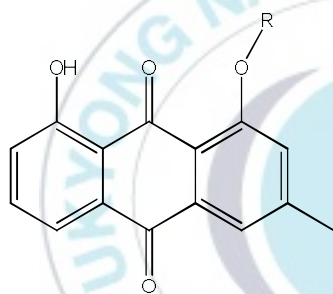


**Physcion 8-*O*- $\beta$ -D-glucopyranoside (8)**



**Toralactone 9-O- $\beta$ -gentiobioside (9)**

**Emodin 1-O- $\beta$ -gentiobioside (10)**



R= glu (1 $\rightarrow$ 6) glu

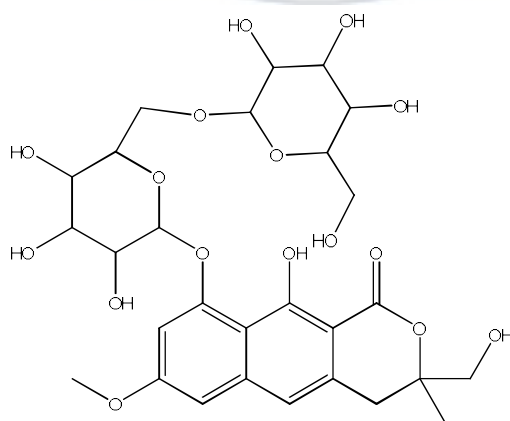
**Chrysophanol 6-O- $\beta$ -D-gentiobioside (12)**

R= glu (1 $\rightarrow$ 6) glu (1 $\rightarrow$ 3) glu

**Chrysophanol 6-O- $\beta$ -D-triglucoside (13)**

R= glu (1 $\rightarrow$ 6) glu (1 $\rightarrow$ 3) glu (1 $\rightarrow$ 6) glu

**Chrysophanol 6-O- $\beta$ -D-tetraglucoside (14)**



**Cassilactone 9-O- $\beta$ -gentiobioside (11)**

Figure 1. Chemical structures of isolated compounds

### **Rubrofusarin (1)**

Orange needles; <sup>1</sup>H-NMR (400 MHz, CD<sub>3</sub>OD) δ: 6.98 (1H, s, H-2), 6.88 (1H, d, *J* = 1.95 Hz, H-8), 6.69 (1H, d, *J* = 1.95 Hz, H-9), 6.04 (1H, s, H-6), 2.38 (3H, s, CH<sub>3</sub>), 3.99 (3H, s, OCH<sub>3</sub>); <sup>13</sup>C-NMR (100 MHz, CD<sub>3</sub>OD) δ: 170.12 (C-2), 106.7 (C-3), 184.2 (C-4), 103.3 (C-4a), 163.1 (C-5), 107.4 (C-5a), 159.5 (C-6), 101.1 (C-7), 163.3 (C-8), 98.5 (C-9), 141.0 (C-10), 101.4 (C-10a), 153.0 (CH<sub>3</sub>), 20.4 and 55.4 (OCH<sub>3</sub>).

### **Rubrofusarin 6-*O*-β-D-glucopyranoside (2)**

Yellow needles; <sup>1</sup>H-NMR (400 MHz, CD<sub>3</sub>OD) δ: 6.86 (1H, s, H-10), 6.80 (1H, d, *J* = 2.1 Hz, H-9), 6.75 (1H, d, *J* = 2.1 Hz, H-7), 6.34 (1H, s, H-3), 5.20 (1H, d, *J* = 7.6 Hz), 3.90 (3H, s, OCH<sub>3</sub>) and 2.56 (3H, s, CH<sub>3</sub>); <sup>13</sup>C-NMR (100 MHz, CD<sub>3</sub>OD) δ: 170.0 (C-2), 110.6 (C-3), 184.5 (C-4), 101.6 (C-4a), 163.0 (C-5), 106.5 (C-5a), 157.7 (C-6), 100.7 (C-7), 163.0 (C-8), 109.7 (C-9), 142.4 (C-9a), 102.0 (C-10), 152.3 (C-10a), 102.0 (C-1'), 75.1 (C-2'), 78.4 (C-3'), 71.2 (C-4'), 78.3 (C-5'), 62.4 (C-6'), 56.0 (OCH<sub>3</sub>), 20.4 (CH<sub>3</sub>).

### **Rubrofusarin 6-*O*-β-D-gentiobioside (3)**

Yellow needles; <sup>1</sup>H-NMR (400 MHz, DMSO-d<sub>6</sub>) δ: 2.39 (3H, s, CH<sub>3</sub>), 3.87 (3H, s, OCH<sub>3</sub>), 4.20 (1H, d, *J* = 8.1 Hz glucosyl H-1), 5.07 (1H, d, *J* = 7.7 Hz, glucosyl H-1), 6.80 (1H, d, *J* = 2.2 Hz, H-7), 6.93 (1H, d, *J* = 2.2 Hz, H-9); <sup>13</sup>C-NMR (100 MHz, DMSO-d<sub>6</sub>) δ: 168.8 (C-2), 106.7 (C-3), 183.7 (C-4), 101.1 (C-4a), 161.9 (C-5), 107.7 (C-5a), 157.6 (C-6), 100.8 (C-7), 161.1 (C-8), 99.7 (C-9), 140.3 (C-9a), 103.6 (C-10), 152.4 (C-10a), 20.2 (CH<sub>3</sub>), 55.5 (OCH<sub>3</sub>), 103.6 (C-1'), 73.5 (C-2'), 76.9 (C-3'), 70.1 (C-4'), 75.5 (C-5'), 68.6 (C-6'), 99.7 (C-1''), 73.5 (C-2''), 76.4 (C-3''), 69.6 (C-4''), 76.7 (C-5''), 61.0 (C-6'').

### **Nor-rubrofusarin 6-*O*-β-D-glucoside (4)**

Yellow powder; <sup>1</sup>H-NMR (400 MHz, DMSO-d<sub>6</sub>) δ: 2.36 (3H, s, CH<sub>3</sub>), 6.12 (1H, s, H-3), 6.72 (1H, d, *J* = 2.0 Hz, H-9), 6.68 (1H, d, *J* = 2.1 Hz, H-7), 7.06 (1H, s, H-10), 5.07 (1H, d, *J* = 7.8 Hz, glucosyl H-1); <sup>13</sup>C-NMR (100 MHz, DMSO-d<sub>6</sub>) δ: 168.6 (C-

2), 106.5 (C-3), 183.7 (C-4), 103.0 (C-4a), 162.1 (C-5), 106.9 (C-5a), 158.3 (C-6), 101.3 (C-7), 159.7 (C-8), 102.5 (C-9), 140.5 (C-9a), 100.0 (C-10), 152.3 (C-10a), 20.1 (CH<sub>3</sub>), 101.2 (C-1'), 73.5 (C-2'), 76.4 (C-3'), 69.6 (C-4'), 77.3 (C-5'), 60.7 (C-6').

#### **Isorubrofusarin 10-*O*- $\beta$ -D-gentiobioside (5)**

Yellow powder; <sup>1</sup>H-NMR (400 MHz, DMSO-d<sub>6</sub>)  $\delta$ : 6.47 (1H, s, H-3), 6.93 (1H, s, H-6), 6.90 (1H, d,  $J$  = 2.1 Hz), 6.80 (1H, d,  $J$  = 2.1 Hz), 4.19 (1H, d,  $J$  = 7.6 Hz, glucosyl H-1), 3.87 (3H, s, OCH<sub>3</sub>), 2.53 (3H, s, CH<sub>3</sub>); <sup>13</sup>C-NMR (100 MHz, DMSO-d<sub>6</sub>)  $\delta$ : 168.35 (C-2), 109.62 (C-3), 182.30 (C-4), 155.59 (C-5), 104.89 (C-6), 99.52 (C-7), 161.10 (C-8), 100.04 (C-9), 156.05 (C-10), 155.15 (C-11), 108.08 (C-12), 140.26 (C-13), 104.89 (C-14), 55.47 (COCH<sub>3</sub>), 19.81 (CH<sub>3</sub>), 99.52 (C-1'), 73.52 (C-2'), 76.89 (C-3'), 70.08 (C-4'), 75.42 (C-5'), 68.69 (C-6'), 103.53 (C-1''), 73.64 (C-2''), 76.65 (C-3''), 69.53 (C-4''), 76.77 (C-5''), 61.04 (C-6'').

#### **Rubrofusarin 6-*O*- $\beta$ -D-triglucoside (6)**

Yellow powder; <sup>1</sup>H-NMR (400 MHz, DMSO-d<sub>6</sub>)  $\delta$ : 2.39 (3H, s, CH<sub>3</sub>), 3.87 (3H, s, OCH<sub>3</sub>), 4.30 (1H, d,  $J$  = 7.5 Hz, glucosyl H-1), 4.32 (1H, d,  $J$  = 7.5 Hz, glucosyl H-1), 5.01 (1H, d,  $J$  = 7.5 Hz, glucosyl H-1), 6.94 (1H, d,  $J$  = 2.2 Hz, H-9), 6.79 (1H, d,  $J$  = 2.2 Hz, H-7), 6.20 (1H, s, H-3), 7.19 (1H, s, H-10); <sup>13</sup>C-NMR (100 MHz, DMSO-d<sub>6</sub>)  $\delta$ : 168.89 (C-2), 106.7 (C-3), 183.8 (C-4), 103.6 (C-4a), 161.9 (C-5), 107.7 (C-5a), 157.6 (C-6), 101.2 (C-7), 161.07 (C-8), 100.8 (C-9), 140.3 (C-9a), 101.2 (C-10), 152.4 (C-10a), 20.2 (CH<sub>3</sub>), 55.5 (OCH<sub>3</sub>), 101.2 (C-1'), 73.4 (C-2'), 76.3 (C-3'), 69.6 (C-4'), 75.6 (C-5'), 68.5 (C-6'), 102.6 (C-1''), 72.2 (C-2''), 88.1 (C-3''), 68.3 (C-4''), 76.0 (C-5''), 60.6 (C-6''), 104.1 (C-1'''), 73.8 (C-2'''), 76.9 (C-3'''), 70.1 (C-4'''), 76.3 (C-5'''), 61.0 (C-6''').

**1-hydroxyl-2-acetyl-3,8-dimethoxynaphthalene-6-*O*- $\beta$ -D-apiofuranosyl-(1 $\rightarrow$ 2)- $\beta$ -D-glucopyranoside (7)**

Yellow powder;  $^1\text{H-NMR}$  (400 MHz, DMSO- $d_6$ )  $\delta$ : 3.90 (3H, s, OCH<sub>3</sub>), 2.85 (3H, s, OCH<sub>3</sub>), 2.54 (3H, s, COCH<sub>3</sub>), 5.23 (1H, d,  $J$  = 5.1 Hz, glucosyl H-1), 6.86 (1H, d,  $J$  = 1.8 Hz, H-5), 6.49 (1H, d,  $J$  = 1.8 Hz, H-7), 6.65 (1H, s, H-4);  $^{13}\text{C-NMR}$  (100 MHz, DMSO- $d_6$ )  $\delta$ : 160.53 (C-1), 109.9 (C-2), 156.1 (C-3), 96.9 (C-4), 102.6 (C-5), 158.5 (C-6), 96.5 (C-7), 159.5 (C-8), 106.4 (C-9), 139.5 (C-10), 55.5 (OCH<sub>3</sub>), 55.9 (CH<sub>3</sub>), 202.6 (COCH<sub>3</sub>), 32.6 (COCH<sub>3</sub>), 98.5 (C-1'), 75.6 (C-2'), 77.0 (C-3'), 69.9 (C-4'), 77.0 (C-5'), 60.5 (C-6'), 108.6 (C-1''), 76.0 (C-2''), 79.3 (C-3''), 74.0 (C-4''), 64.4 (C-5'').

**Physcion 8-*O*- $\beta$ -D-glucopyranoside (8)**

Orange powder;  $^1\text{H-NMR}$  (600 MHz, DMSO- $d_6$ )  $\delta$ : 2.40(3H, s, CH<sub>3</sub>), 3.95(3H, s, OCH<sub>3</sub>), 2.90(1H, s, H-4), 5.15(1H, d,  $J$  = 7.5 Hz, glucosyl H-1), 7.47 (1H, s, H-4), 7.35 (1H, d,  $J$  = 2.7 Hz, H-5), 7.17 (3H, d,  $J$  = 2.1 Hz, H-7);  $^{13}\text{C-NMR}$  (100 MHz, DMSO- $d_6$ )  $\delta$ : 161.6 (C-1), 124.1 (C-2), 147.0 (C-3), 119.3 (C-4), 107.3 (C-5), 164.6 (C-6), 106.5 (C-7), 160.6 (C-8), 186.4 (C-9), 181.8 (C-10), 136.0 (C-11), 114.4 (C-12), 114.4 (C-13), 132.0 (C-14), 21.6 (CH<sub>3</sub>), 56.0 (OCH<sub>3</sub>), 100.7 (C-1'), 73.2 (C-2'), 76.5 (C-3'), 69.7 (C-4'), 77.4 (C-5'), 60.7 (C-6').

**Emodin 1-*O*- $\beta$ -gentiobioside (10)**

Brownish red powder;  $^1\text{H-NMR}$  (400 MHz, DMSO- $d_6$ )  $\delta$ : 2.47 (3H, s, CH<sub>3</sub>), 4.20 (1H, d,  $J$  = 7.6 Hz, glucosyl H-1), 5.11 (1H, d,  $J$  = 7.3 Hz, glucosyl H-1), 7.04 (1H, d,  $J$  = 2.5 Hz, H-5), 6.55 (1H, d,  $J$  = 2.2 Hz, H-7), 7.57 (1H, s, H-2), 7.67 (1H, s, H-4);  $^{13}\text{C-NMR}$  (100 MHz, DMSO- $d_6$ )  $\delta$ : 158.2 (C-1), 123.3 (C-2), 146.7 (C-3), 121.5 (C-4), 1334.0 (C-4a), 107.6 (C-5), 165.3 (C-6), 108.2 (C-7), 164.6 (C-8), 109.8 (C-8a), 185.9 (C-9), 182.3 (C-10), 134.2 (C-10a), 21.7 (CH<sub>3</sub>), 103.7 (C-1'), 73.6 (C-2'), 76.6 (C-3'), 70.1 (C-4'), 75.8 (C-5'), 69.0 (C-6'), 100.7 (C-1''), 73.4 (C-2''), 76.3 (C-3''), 69.7 (C-4''), 76.9 (C-5''), 61.0 (C-6'').

**(3*R*)-cassilactone 9-*O*- $\beta$ -D-gentiobioside (11)**

Orange color powder; <sup>1</sup>H-NMR (600 MHz, DMSO-d<sub>6</sub>)  $\delta$ : 1.28(3H, s, CH<sub>3</sub>), 3.86(3H, s, OCH<sub>3</sub>), 2.90(1H, s, H-4), , 5.03(1H, d,  $J$  = 8.2 Hz, glucosyl H-1), 4.19(1H, d,  $J$  = 7.6 Hz, glucosyl H-1 ), 6.86 (3H, d,  $J$  = 2.1 Hz, H-6), 6.87 (3H, d,  $J$  = 2.04 Hz, H-8) ; <sup>13</sup>C-NMR (100 MHz, DMSO-d<sub>6</sub>)  $\delta$ : 169.7 (C-1), 83.8 (C-3), 33.7 (C-4), 133.6 (C-4a), 115.7 (C-5), 140.7 (C-5a), 100.2 (C-6), 161.1 (C-7), 101.7 (C-8), 157.7 (C-9), 109.8 (C-9a), 21.6 (CH<sub>3</sub>), 55.4 (OCH<sub>3</sub>), 66.3 (OCH<sub>3</sub>), 103.5 (C-1'), 73.4 (C-2'), 76.6 (C-3'), 70.0 (C-4'), 75.5 (C-5'), 68.7 (C-6'), 101.0 (C-1''), 73.5 (C-2''), 76.3 (C-3''), 69.6 (C-4''), 76.8 (C-5''), 61.0 (C-6'').



#### **4-2. *In vitro* ChEs enzyme assay**

The inhibitory activities of isolated compounds against ChEs were measured using the spectrophotometric method reported by Ellman et al. (1961). Briefly, ACh and BCh were used as the substrates to assay the inhibition of AChE and BChE, respectively. Each reaction mixture contained 140  $\mu\text{l}$  of sodium phosphate buffer (pH 8.0); 20  $\mu\text{l}$  of compounds (final conc., 100  $\mu\text{M}$ ); and 20  $\mu\text{l}$  of either AChE or BChE solution, which was mixed and incubated for 15 min at room temperature. Compounds and the positive control (berberine) were dissolved in 10% analytical grade DMSO. Reactions were initiated by the addition of 10  $\mu\text{l}$  of DTNB and 10  $\mu\text{l}$  of either ACh or BCh. The hydrolysis of ACh or BCh was monitored by following the formation of the yellow 5-thio-2-nitrobenzoate anion at 412 nm for 15 min, which was generated via reaction of DTNB with thiocholine and released from the respective enzymatic hydrolysis by either ACh or BCh. All reactions were performed in triplicate and recorded in 96-well microplates, using a microplate spectrophotometer (Molecular Devices, Sunnyvale, CA, USA). Percent inhibition was calculated as  $(1-S/E) \times 100$ , where E and S were the respective enzyme activities without and with the tested sample, respectively. ChEs inhibitory activities were expressed in terms of the  $\text{IC}_{50}$  value ( $\mu\text{M}$  required to inhibit hydrolysis of the substrate, ACh or BCh, by 50%) as calculated from the log-dose inhibition curve. Berberine was used as a positive control.

### 4-3. BACE1 inhibitory assay

Each assay was carried out according to the supplied instructions with selected modifications. Briefly, mixtures of 10  $\mu$ l of assay buffer (50 mM sodium acetate, pH 4.5), 10  $\mu$ l of BACE1 (1.0 U/ml), 10  $\mu$ l of the substrate (750 nM Rh-EVNLDAEFK-Quencher in 50 mM ammonium bicarbonate), and 10  $\mu$ l of compounds (final conc., 100  $\mu$ M) dissolved in 10% DMSO were incubated for 60 min at 25°C in the dark. The proteolysis of two fluorophores (Rh-EVNLDAEFK-Quencher) by BACE1 was monitored by the formation of fluorescent donor Rh-EVNL (530–545 nm, excitation; 570–590 nm, emission), the abundance of which was determined by measuring the increase in fluorescence excited at 545 nm and recorded at 585 nm. Fluorescence was measured with a microplate spectrofluorometer (Gemini EM, Molecular Devices, CA, USA). The percent inhibition (%) was obtained by the following equation: % Inhibition =  $[1 - (S_{60} - S_0) / (C_{60} - C_0)] \times 100$ , where  $C_{60}$  was the fluorescence of the control (enzyme, buffer, and substrate) after incubation for 60 min,  $C_0$  was the initial fluorescence of the control,  $S_{60}$  was the fluorescence of the tested samples (enzyme, sample solution, and substrate) after incubation for 60 min, and  $S_0$  was the initial fluorescence of the tested samples. To account for the quenching effect of samples, the sample solution was added to a separate reaction mixture C, and any reduction in fluorescence by the sample was investigated. The BACE1 inhibitory activity of compounds was expressed in terms of the  $IC_{50}$  value ( $\mu$ M required to inhibit proteolysis of the substrate, BACE1, by 50%), as calculated from the log-dose inhibition curve. Quercetin was used as a positive control.

#### **4-4. Enzyme kinetic analysis with BChE and BACE1**

To examine the kinetics of rubrofusarin 6-*O*- $\beta$ -D-gentiobioside/AChE and nor-rubrofusarin 6-*O*- $\beta$ -D-glucoside/BACE1 interaction, we employed two complementary kinetic methods, namely Lineweaver–Burk and Dixon plots (Lineweaver et al., 1934, Dixon et al., 1953). Specifically, Dixon plots for AChE and BACE1 inhibition by rubrofusarin 6-*O*- $\beta$ -D-gentiobioside and rubrofusarin 6-*O*- $\beta$ -D-glucoside, respectively, were achieved in the presence of different substrate concentration (0 to 0.1 mM for AChE and 0 to 750 nM for BACE1). Inhibition constants ( $K_i$ ) were determined by interpretation of Dixon plots, where the x-axis intercept was taken as  $K_i$ . The enzyme assays were performed using previously mentioned methods.

#### **4-5. Molecular docking simulation**

##### **4-5-1. Molecular docking simulation in AChE inhibition**

The crystal structures of the AChE protein target was acquired from the RCSB Protein Data Bank (PDB) with the accession codes 1acj. The co-crystallized ligands, tacrine (THA) and donepezil were used to generate the grid box for catalytic and allosteric inhibition mode respectively (Kryger et al., 1997). The binding AChE inhibitor and water molecules were removed from the structure for the docking simulation using Accelrys Discovery Studio 4.1 (Accelrys, Inc. San Diego, CA, USA). The 3D structures of rubrofusarin and its derivatives were drawn with ChemDraw Ultra 12.0 (CambridgeSoft, Cambridge, MA, USA) and their pKa values were computed at crystallographic pH (pH = 7.5) using the MarvinSketch (ChemAxon, Budapest, Hungary). Automated docking simulations was performed using Autodock Tools (ADT) to assess the appropriate binding orientations and conformations of the AChE with the different compounds. A Lamarkian genetic algorithm method in Autodock 4.2 was employed. For docking calculations, Gasteiger charges were added by default, the

rotatable bonds were set by the ADTs, and all torsions were allowed to rotate. The grid maps were generated by the Autogrid program. The binding aspect of AChE residues and their corresponding binding affinity score were regarded as the best molecular interaction. PyMOL 1.7.4 and Ligplot+ were used for visualization and analysis of results.

#### **4-5-2. Molecular docking simulation in BACE1 inhibition**

X-ray crystallographic structure of BACE 1 (PDB ID: 2wjo), with its potent inhibitors 2-amino-3-((1R)-1-cyclohexyl-2-[(cyclohexylcarbonyl)amino]ethyl)-6-phenoxyquinazolin-3-ium (QUD) and 3,5,7,3',4'-pentamethoxyflavone (PMF) were obtained from RCSB Protein Data Bank (PDB). The binding BACE1 inhibitor and water molecules were removed from the structure for the docking simulation using Accelrys Discovery Studio 4.1 (Accelrys, Inc. San Diego, CA, USA). The 3D structures of rubrofusarin and its derivatives were drawn with ChemDraw Ultra 12.0 (CambridgeSoft, Cambridge, MA, USA) and their pKa values were computed at crystallographic pH (pH = 7.5) using the MarvinSketch (ChemAxon, Budapest, Hungary). Automated docking simulations was performed using Autodock Tools (ADT) to assess the appropriate binding orientations and conformations of the AChE with the different compounds. A Lamarckian genetic algorithm method in Autodock 4.2 was employed. For docking calculations, Gasteiger charges were added by default, the rotatable bonds were set by the ADTs, and all torsions were allowed to rotate. The grid maps were generated by the Autogrid program where the grid box size of  $80 \times 80 \times 80$  had a default spacing of 0.375 Å. The binding aspect of AChE residues and their corresponding binding affinity score were regarded as the best molecular interaction. PyMOL 1.7.4 and Ligplot+ were used for visualization and analysis of results.

## 5. Statistical analysis

The significant of differences between the control and test groups were determined by statistical testing using Student's *t*-test (Sysat In., Evaston, IL, USA), and  $P < 0.05$  was used as the cutoff for statistical significance. All results are presented as the mean  $\pm$  S.E.M. of triplicate experiments.



## . Results

### 1. Inhibitory activities of rubrofusarin and its derivatives against AChE, BChE and BACE1

In order to evaluate the anti-AD potential of the isolated rubrofusarin and its five derivatives, we evaluated their abilities to inhibit AChE, BChE and BACE1. Results are summarized in Table 1. Of the derivatives, **3** showed most potent activity against AChE with an  $IC_{50}$  of  $15.94 \pm 0.32 \mu\text{M}$  whereas **2** had least inhibitory activity ( $148.08 \pm 2.09 \mu\text{M}$ ). **4**, **5**, and **6** exhibited moderate inhibition with  $IC_{50}$  value of  $86.05 \pm 2.01$ ,  $83.52 \pm 1.56$ , and  $82.31 \pm 1.63 \mu\text{M}$ , respectively, compared with the positive control berberine ( $0.68 \pm 0.01 \mu\text{M}$ ). Next, we investigated the BChE inhibitory activities of rubrofusarin and its derivatives. Unfortunately, only **3** inhibited BChE with an  $IC_{50}$  value of  $141.15 \pm 1.23 \mu\text{M}$ . Finally, the selected compounds were investigated for their activity against BACE1. Interestingly, **4** (methoxyl group substituted by hydroxyl at C-8 position) was most potent with an  $IC_{50}$  value of  $14.41 \pm 2.87 \mu\text{M}$  (the positive control quercetin had an  $IC_{50}$  value of  $21.42 \pm 1.04$ ). **1** and **3** demonstrated moderate inhibition with  $IC_{50}$  value of  $90.01 \pm 2.38$  and  $85.66 \pm 3.98 \mu\text{M}$ , respectively. However, **5** (an isomer of **3**) and **6** demonstrated no significant inhibitory activity at concentration up to  $200 \mu\text{M}$ .

## 2. Enzyme kinetic analysis of active compounds with AChE and BACE1

Since compound **3** showed high AChE inhibitory activity, it was subjected to an enzyme kinetic study. According to the Lineweaver-Burk plot (Fig. 2), it exhibited mixed type inhibition against AChE. Moreover, the Dixon plot revealed a  $K_i$  value of 12.83  $\mu\text{M}$ . Since **4** showed significantly high inhibitory activity against BACE1, it was also subjected to an enzyme kinetic study (Fig. 3). Its Dixon plot revealed a  $K_i$  value of 10.01  $\mu\text{M}$ . The results of the enzyme kinetic analysis of **3** and **4** against AChE and BACE1 are shown in Table 1. In general, compounds with lower  $K_i$  value are preferred and are more active inhibitors against AChE and BACE1 ( $K_i$  value indicates the concentration of inhibitor required to combine with the enzyme).

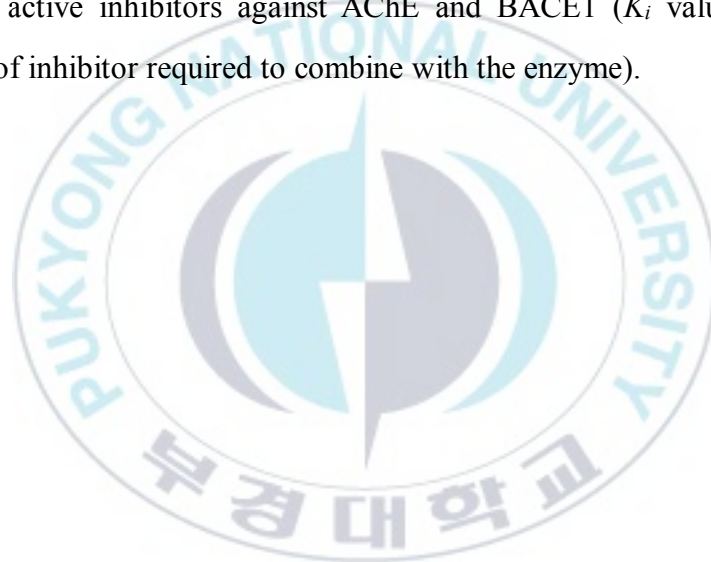


Table 1. Cholinesterase and BACE1 inhibitory activity of compounds isolated from *Cassia obtusifolia*

Compounds	AChE	BChE	BACE1	$K_i$ value	Inhibition type
	IC <sub>50</sub> (μM) <sup>a</sup>				
<b>1</b>	124.13 ± 1.39	>200	90.01 ± 2.38	-	-
<b>2</b>	148.08 ± 2.09	>200	190.63 ± 4.68	-	-
<b>3</b>	15.94 ± 0.32	141.15 ± 1.23	85.66 ± 3.98	12.83 <sup>b</sup>	Mixed type <sup>c</sup>
<b>4</b>	86.05 ± 2.01	>200	14.41 ± 2.87	10.01 <sup>d</sup>	Mixed type <sup>e</sup>
<b>5</b>	83.52 ± 1.56	>200	>200	-	-
<b>6</b>	82.31 ± 1.63	>200	>200	-	-
Berberine <sup>f</sup>	0.68 ± 0.01	25.77 ± 0.26	-	-	-
Quercetin <sup>f</sup>	-	-	21.42 ± 1.04	-	-

<sup>a</sup> The 50% inhibitory concentration (IC<sub>50</sub>) values (μM) were calculated from a log dose inhibition curve and expressed as mean ± S.E.M of triplicate experiments.

<sup>b,d</sup> AChE and BACE1 inhibition constants (K<sub>i</sub>), respectively, were determined using a Dixon plot.

<sup>c,e</sup> AChE and BACE1 inhibition type, respectively, were determined using Dixon and Lineweaver-Burk plots.

<sup>f</sup> Positive controls.

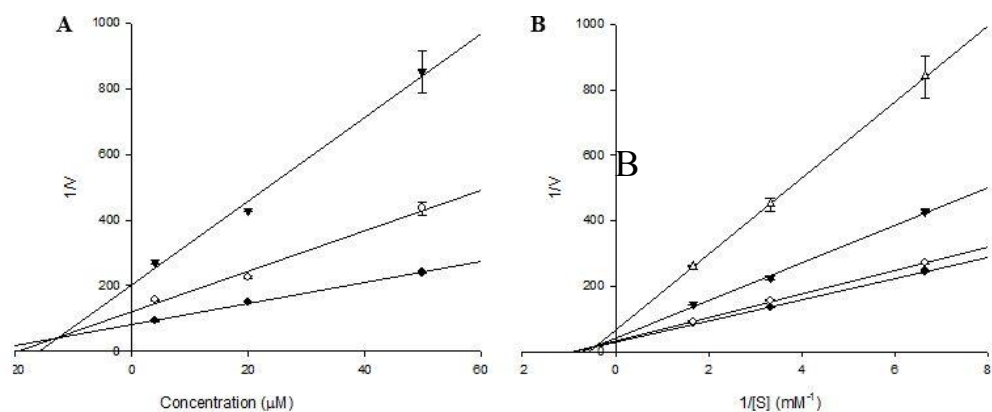


Figure 2. Dixon plots and Lineweaver-Burk plots for AChE inhibition by **3**. The results showed the effects of presence of different concentrations of the substrate (0.6 (●), 0.3 (○), and 0.1 mM (▼)) for (A) and the effect of presence of different concentrations of **3** (0 (●), 4 (○), 20 (▼), and 50  $\mu$ M ( $\Delta$ )) for (B).

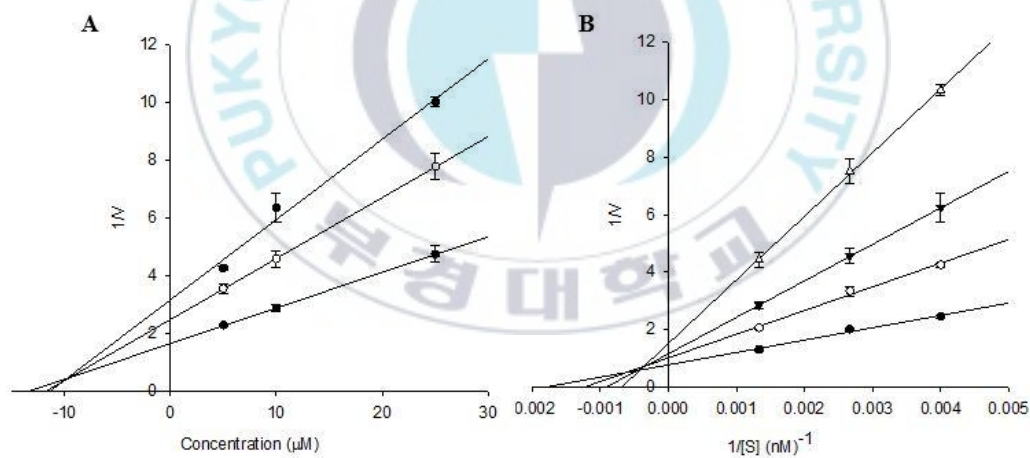


Figure 3. Dixon plots and Lineweaver-Burk plots for BACE1 inhibition by **4**. The results showed the effects of presence of different concentrations of the substrate (252 (●), 375 (○), and 750 nM (▼)) for (A) and the effect of presence of different concentration of **4** (0 (●), 5 (○), 10 (▼), and 25  $\mu$ M ( $\Delta$ )) for (B).

### 3. Molecular docking simulation in AChE inhibition

Molecular docking models of **3** and tacrine are illustrated in Fig. 4. Molecular docking simulation provides a means of understanding protein–ligand interaction geometrics at a molecular level. Tacrine and donepezil were used as a standard ligand to validate the Autodock 4.2 results. The binding energy of **1-3** with interacting residues including H-bond interacting residues and van der Waals interacting residues along with the number of H-bonds are listed in Table 2. AChE-rubrofusarin 6-*O*- $\beta$ -D-gentiobioside complex had a  $-9.06$  kcal/mol binding energy having seven H-bonds with interacting residues of TYR70, ASN85, SER122, GLU199 and HIS440 (Fig. 4B) in case of mixed-mode inhibition. The hydroxyl and oxygen group of TYR70 formed hydrogen bonds with the oxygen and hydroxyl group of **3**, with bond distances of 3.28 and 3.21 Å, respectively. The other groups involved in hydrogen bonding were the oxygen of ASN85, SER122, and HIS440 with the hydroxyl group of **3** (bond distances of 2.88, 2.66, and 2.64 Å, respectively). Additionally, two H-bonds were observed between the GLU199 (oxygen group) and **3** (hydroxyl group) with bond distances of 2.54 and 2.86 Å, respectively. In addition, hydrophobic interactions were also observed between VAL71, ASP72, GLN74, TRP84, GLY117, GLY118, TYR121, SER200, PHE290, PHE330, PHE331, TYR334, and GLY441 residues.

Autodock 4.2 simulations results for interactions between the **1-3** or donepezil with AChE are illustrated in Fig. 5. The results demonstrated that AChE-rubrofusarin complex at the allosteric site has three H-bonding interactions between GLN69 and TYR70 residues of enzyme and **1** ( $-7.95$  kcal/mol binding energy) through bond distances of 2.73, 3.11, and 2.82 Å, respectively. Furthermore, ASP72, TRP84, ASN85, PRO86, GLY117, GLY118, TYR121, SER122, GLY123, LEU127, and TYR130 of AChE were participated in hydrophobic interactions (Figs. 5A and 5D). Similarly, AChE-rubrofusarin 6-*O*- $\beta$ -D-glucopyranoside complex had a binding energy of  $-7.51$  kcal/mol and five H-bonds due to interactions with residues TYR121, TYR334, PHE288, and ARG289 with bond distances of 3.16, 3.28, 2.99, 2.85, and 3.24 Å, respectively. In addition, **2** showed hydrophobic interactions with TYR70, ASP72,

TRP279, SER286, ILE287, PHE290, PHE330, and PHE331 of AChE (Figs. 5B and 5E). Interestingly, AChE-rubrofusarin 6-*O*- $\beta$ -D-gentiobioside complex had a  $-9.57$  kcal/mol binding energy and formed three hydrogen bonds with TYR70, ASN85 and TYR121 (Fig. 4). Hydrogen bonding was observed by the oxygen group of TYR70, ASN85 and TYR121 and the hydroxyl group of **3** with the bond distance of 2.59, 3.16 and 3.27 Å, respectively. In addition, VAL71, ASP72, GLY80, SER81, TRP84, GLY118, GLY119, SER122, SER200, TRP279, ILE287, PHE330, PHE331, TYR334, GLY335, TRP432, ILE439, HIS440, and TYR442 of AChE participated in hydrophobic interactions (Fig. 4B).



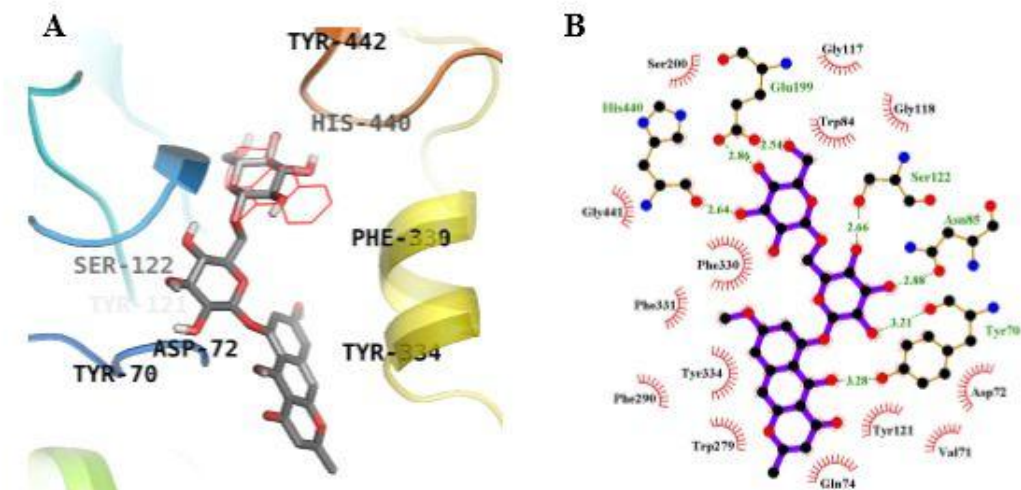
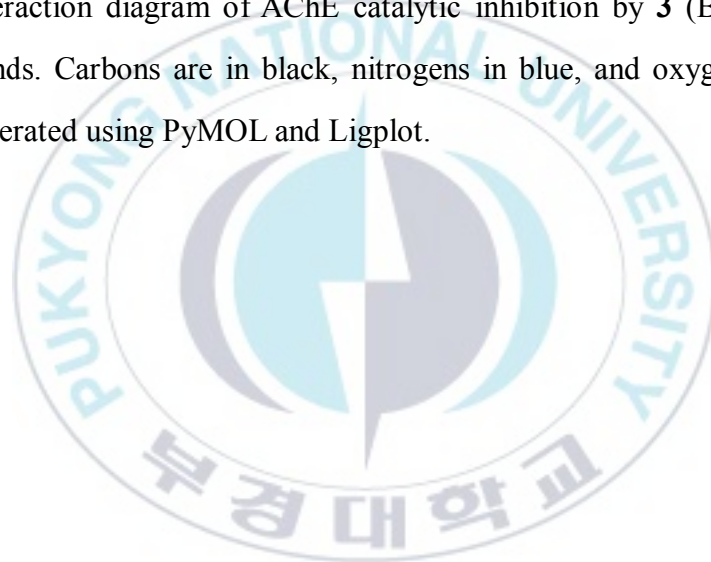


Figure 4. Inhibition mode of **3** (A) for the AChE active site with tacrine (*red stick*) (A). 2D ligand interaction diagram of AChE catalytic inhibition by **3** (B). Dashed lines indicate H-bonds. Carbons are in black, nitrogens in blue, and oxygens in red. The figure was generated using PyMOL and Ligplot.



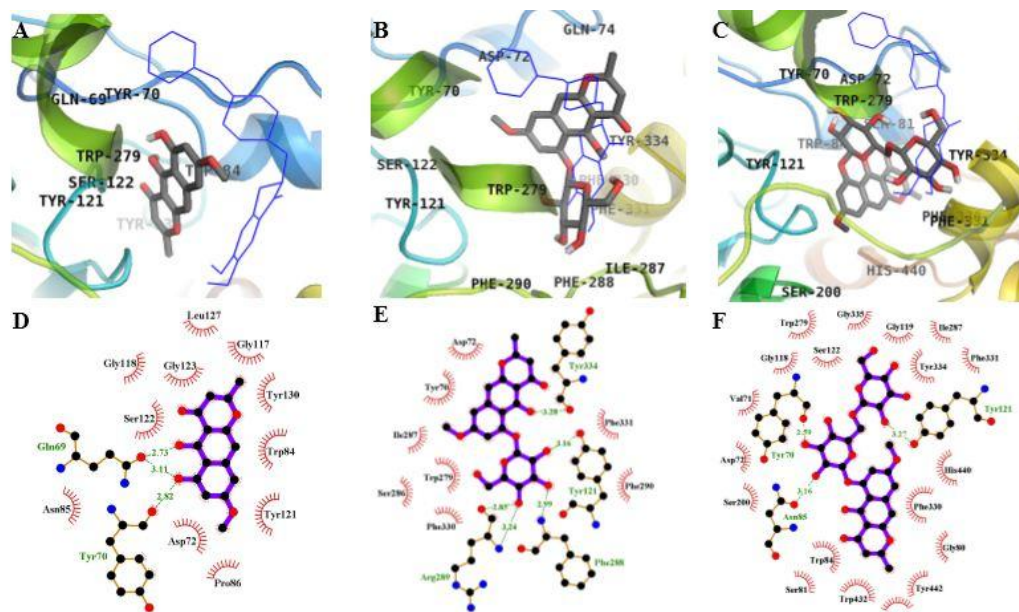


Figure 5. Inhibition mode of **1** (A), **2** (B), and **3** (C) for the AChE allosteric site with donepezil (*blue stick*) (A). 2D ligand interaction diagram of AChE allosteric inhibition by **1** (D), **2** (E), and **3** (F). Dashed lines indicate H-bonds. Carbons are in black, nitrogen in blue, and oxygen in red. The figure was generated using PyMOL and Ligplot.

Table 2. Docking affinity scores and possible H-bond formation to AChE (1acj) active sites by **1**, **2**, and **3** along with reported inhibitors

Compounds	Autodock 4.2 Score (Kcal/mol) <sup>a</sup>	No. of H-bonds	H-bonds interacting residues <sup>b</sup>	van der Waals interacting residues <sup>b</sup>
<b>1</b> (Allosteric inhibition mode)	-7.95	3	Gln69, Tyr70	Asp72, Trp84, Asn85, Pro86, Gly117, Gly118, Tyr121, Ser122, Gly123, Leu127, Tyr130
<b>2</b> (Allosteric inhibition mode)	-7.51	5	Tyr121, Arg289, Tyr334, Phe288	Tyr70, Asp72, Trp279, Ser286, Ile287, Phe290, Phe330, Phe331
<b>3</b> (Mixed inhibition mode)	-9.06	7	Tyr70, Asn85, Ser122, Glu199, His440	Val71, Asp72, Gln74, Trp84, Gly117, Gly118, Tyr121, Ser200, Phe290, Phe330, Phe331, Tyr334, Gly441
<b>3</b> (Allosteric inhibition mode)	-9.57	3	Tyr70, Asn85, Tyr121	Val71, Asp72, Gly80, Ser81, Trp84, Gly118, Gly119, Ser122, Ser200, Trp279, Ile287, Phe330, Phe331, Tyr334, Gly335, Trp432, Ile439, His440, Tyr442
Tacrine <sup>c</sup> (Catalytic inhibitor)	-9.8	1	His440	Tyr442, Phe330, Trp84, Gly118, Trp432, Gly441, Tyr334, Glu199
Donepezil <sup>c</sup> (Allosteric inhibitor)	-10.6	-	-	Tyr70, Ile275, Asp276, Trp279, Ile287, Phe288, Arg289, Tyr334, Tyr121, Ser286, Phe290, Phe330, Phe331

<sup>a</sup> Binding energy, which indicates binding affinity and capacity for the active site of the AChE enzyme. <sup>b,c,d</sup> The number of hydrogen bonds and all amino acid residues from the enzyme-inhibitor complex were determined with the AutoDock 16.1 program.

#### 4. Molecular docking simulation in BACE1 inhibition

The binding energy of **4** and **2** with the interacting residues, including H-bond interacting residues and van der Waals interactions, and numbers of H-bonds are listed in Table 3. QUD (catalytic inhibitor) and PMF (allosteric inhibitor) were used as positive ligands. According to Autodock 4.2 simulation results (Fig. 6), the BACE1-nor-rubrofusarin 6-*O*- $\beta$ -D-glucoside complex had a binding energy of  $-6.61$  Kcal/mol with six H-bonds at ASP32, TRP76, ASN37, ILE126, and TYR198 (Fig. 6C) as was observed in catalytic inhibition mode. Ile126 formed two H-bonds with the hydroxyl group of **4** with bond distances of 2.54 and 2.93 Å, respectively. In addition, H-bonding was observed between oxygen group of TYR198, ASN37, TRP76, and ASP32 and the hydroxyl group of **4** with bond distance of 3.06, 2.75, 3.09, and 2.88 Å, respectively. Further, GLY230, GLY34, VAL69, PHE108, ASP106, LYS75, PRO70, TYR71, SER35, and ARG128 also exhibited hydrophobic interactions. Similarly, **2** bound to catalytic site of BACE1 with binding energy of  $-5.38$  Kcal/mol and formed four H-bonds with TRP76, LYS107, PHE108 with bond distances of 2.77 Å, 3.02 Å, 2.80 Å, and 2.84 Å, respectively (Fig. 6D). ASP32, GLY34, SER35, ASN37, VAL69, ILE110, TRP115, ILE118, ARG128, ASP228, GLY230, and THR231 were found to contribute in hydrophobic interactions.

On the other hand, the BACE1-nor-rubrofusarin 6-*O*- $\beta$ -D-glucoside complex had a binding energy of  $-8.34$  Kcal/mol and formed six H-bonds with GLN303, GLN304, GLU339, and GLY156 in allosteric inhibition mode (Fig.7). SER10, ALA335, VAL170, TYR14, GLY13, GLY11, THR232, ARG307, VAL336, VAL361, ALA157, and PRO308 were found to participate in hydrophobic interactions.

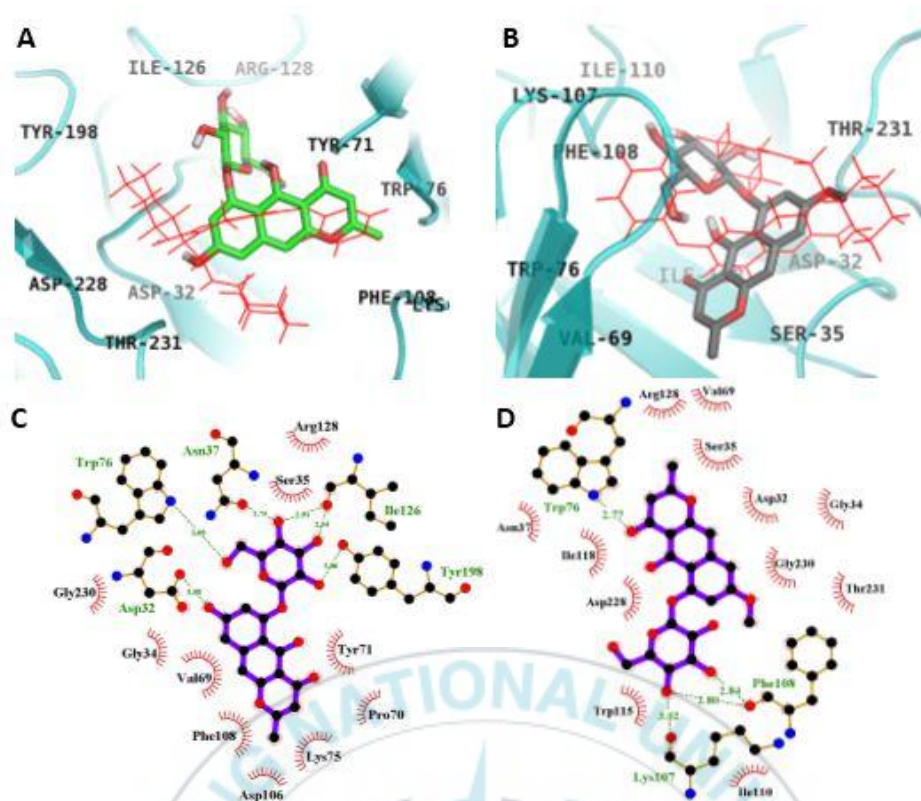


Figure 6. Inhibition mode of **4** (A) and **2** (B) for the BACE1 catalytic site with QUD (*red stick*) (A). 2D ligand interaction diagrams of BACE1 catalytic inhibition by **4** (C) and **2** (D). Dashed lines indicate H-bonds. Carbons are in black, nitrogens in blue, and oxygen in red. The figure was generated using PyMOL and Ligplot.

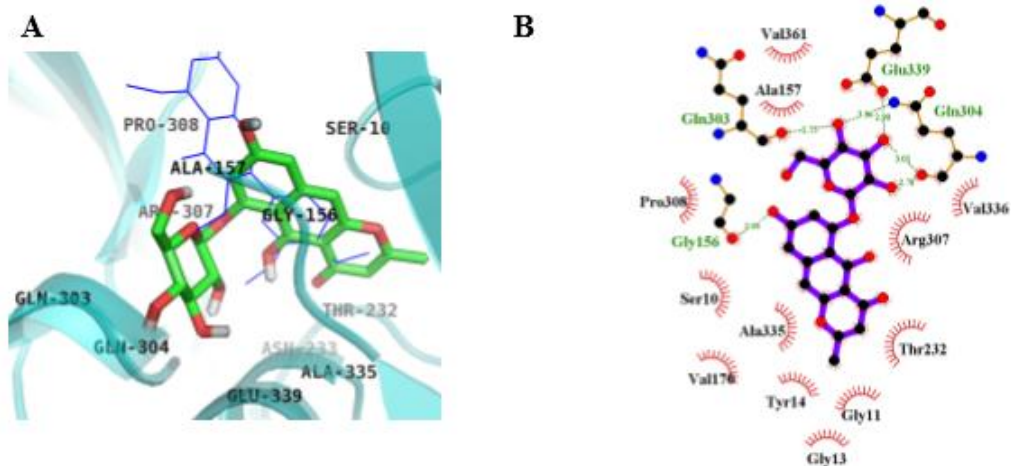


Figure 7. Inhibition mode of **4** for the BACE1 allosteric site with PMF (*blue stick*) (A). 2D ligand interaction diagram of BACE1 allosteric (B) inhibition by **4**. Dashed lines indicate H-bonds. Carbons are in black, nitrogens in blue, and oxygens in red. The figure was generated using PyMOL and Ligplot.

Table 3. Docking affinity scores and possible H-bond formation to BACE1 (2wjo) active sites by **4** and **2** along with reported inhibitors

Compounds	Autodock 4.2 Score (Kcal/mol) <sup>a</sup>	No. of H-bonds	H-bonds interacting residues <sup>b</sup>	van der Waals interacting residues <sup>b</sup>
<b>4</b> (Catalytic inhibition mode)	-6.61	6	Asp32, Trp76, Asn37, Ile126, Tyr198	Gly230, Gly34, Val69, Phe108, Asp106, Lys75, Pro70, Tyr71, Ser35, Arg128
<b>4</b> (Allosteric inhibition mode)	-8.34	6	Gln303, Gln304, Glu339, Gly156	Ser10, Ala335, Val170, Tyr14, Gly13, Gly11, Thr232, Arg307, Val336, Val361, Ala157, Pro308
<b>2</b> (Catalytic inhibition mode)	-5.38	4	Trp76, Lys107, Phe108	Asp32, Gly34, Ser35, Asn37, Val69, Ile110, Trp115, Ile118, Arg128, Asp228, Gly230, Thr231
QUD <sup>c</sup> (Catalytic inhibitor)	-9.3	4	Asp228, Asp32, Gly230	Lys107, Lys75, Gly74, Leu30, Thr231, Val69, Tyr198, Ile226, Thr329, Gly34, Arg235, Ser35, Tyr71, Ile118
PMF <sup>c</sup> (Allosteric inhibitor)	-6.5	1	Ser10	Gly11, Ala157, Ala168, Val170, Thr232, Gln304, Arg307, Pro308, Tyr320, Ala335, Glu339

<sup>a</sup> Estimated the binding free energy of the ligand receptor complex. <sup>b</sup> All amino acid residues located 5 Å from the original enzyme/compound complex in the AutoDock 4.2 program. <sup>c</sup> Positive ligands. .

## . Discussion

Considerable research efforts have been directed towards discovering the cause of AD in recent years with the ultimate hope of developing safe and effective pharmacological treatments. Symptoms control, maintaining functional status, improving quality of life, minimizing the adverse drug effect and reducing caregiver stress are the main management target in AD. ACh, a neurotransmitter plays an essential role in memory and learning, and AChE is the enzyme that hydrolyze ACh at the cholinergic synapses in the central and peripheral nervous system. AChE inhibitors promote an increase in the concentration and the duration of action of synaptic ACh and thus, enhance cholinergic transmission through the activations of synaptic nicotinic and muscarinic receptors. Reports suggest AChE plays a key role during the early development of senile plague, as was revealed by the finding that AChE accelerates  $\beta$ -amyloid peptide ( $A\beta$ ) deposition (Inestrosa et al., 1996). Second generation ChEs inhibitors like donepezil, rivastigmine, metrifonate and galantamine are now used for the symptomatic relief of AD, and provide benefits at least as great as those reported for tacrine, but with more favorable clinical profiles (Francis et al., 1999). The AChE inhibitors donepezil and rivastigmine have similar mode of action (both increase the concentration of Ach at the neurotransmitter sites). Galantamine also acts in the same manner but also modulates activity at the nicotinic receptor (Tricco et al., 2012). Nevertheless, available drugs have side effects, like gastro-intestinal (GI) disturbances, nausea, vomiting, and diarrhea and also have bioavailability issues (Schulz et al., 2003). Nowadays, natural medicinal drugs are reclaiming their position as the primary source of treatment as alternatives to synthetic agents (Cerella et al., 2014, Gechev et al., 2014, Georgiev et al., 2014, Schnekenburger et al., 2014). Research on *C. obtusifolia* indicates it has beneficial effects in AD, diabetes, and Parkinson's disease and that it acts as a hepatoprotective and antioxidant.

The sugar moiety attached to a specific position on the aglycone core plays an

important role in structural biodiversity of natural products. These sugar components usually participate in the molecular recognition of its cellular target, and thus, they are important for biological activity. These sugars can be linked to an aglycone as monosaccharides, disaccharides or oligosaccharides of variable sugar lengths via *C*-, *N*- or *O*-glycosylation (the latter is the most common) (Weymouth-Wilson et al., 1997). In addition, several reports have been issued on the influence of methoxyl group on biological activity (Metwally et al., 2013, Sato et al., 2014, Yanagita et al., 2013).

In the present study, we investigated the anti-AD activity of rubrofusarin and its derivatives isolated from *C. obtusifolia* by performing ChEs and BACE1 inhibitory assay (Table 1). All six tested compounds showed promising inhibitory activity against AChE with IC<sub>50</sub> ranging from 15.94 to 148.08 μM. The abilities of five selected compounds to inhibit AChE followed in decreasing order, **3** > **6** > **5** > **4** > **1** > **2**, respectively. Interestingly, **3** which contains two sugar moieties, inhibited AChE nine times more effectively, than **2** (having one sugar moiety), eight times more than **1** (having no sugar moiety), and five times than **5** (an isomer of **3**), **6** and **4**, respectively. Examination of the SAR of rubrofusarin and its derivatives isolated from *C. obtusifolia* indicated that introduction of gentiobiosyl moiety in the **1** (IC<sub>50</sub> = 124.13 μM) scaffold (**3** (IC<sub>50</sub> = 15.94 μM)) increased AChE inhibitory activity whereas addition of one more glucose in **3** (**6** (IC<sub>50</sub> = 82.31 μM)) decreases AChE inhibitory activity, indicating the importance of gentiobiosyl moiety and the length of sugar moiety at C-6. This results shows that gentiobiosyl moiety may be the optimum sugar length for the particular biological activity. By comparing AChE inhibitory activity of **3** with its isomer **5** (IC<sub>50</sub> = 83.52 μM) which differs with respect to the arrangement of pyrone ring in the naphthalene group (i.e. the pyrone ring attached at β-position at naphthalene ring in **5** and at γ-position in **3**) revealed that arrangement of pyrone at naphthalene ring and sugar position greatly influence activity. In addition, introduction of hydroxyl group at C-8 position of **2** (IC<sub>50</sub> = 148.08 μM) in **4** (IC<sub>50</sub> = 86.05 μM) increased the inhibitory activity, indicating the importance of hydroxyl group at C-8 position for its activity. Similar results regarding the correlation between methoxyl group at C-6/C-7/C-8

position and AChE inhibitory activity was also obtained in our previous study (Ali et al., 2016). A relation between the presences of C-1 methoxyl group in the new series of aryl-naphthalenes with the decrease in antitumor activity has been previously reported (Luo et al., 2014).

In order to support the SARs of compounds obtained from experimental data and to evaluate the binding site-directed inhibition of AChE; kinetic and docking studies were performed. Molecular docking simulation is a potent and progressively important tool for drug discovery (Meng et al., 2011, Morris et al., 2008) and can be used for screening and identification of probable biological active chemical moiety from natural product databases (Ma et al., 2011). We obtained docking score using Autodock 4.2 to estimate the strength of the different protein-ligand complex interaction. For the docking studies, we used tacrine and donepezil as catalytic and allosteric inhibitor, respectively to validate the results for AChE. These studies reveal that **3** exhibited mixed type of inhibition whereas **1** and **2** exhibited allosteric type inhibition. Molecular docking of **3** produced an unanticipated result. Generally, mixed type of inhibition implies binding with catalytic and allosteric site, however, docking at the catalytic site revealed, the presence of allosteric and catalytic interacting residues suggesting the compound's preference for allosteric site over catalytic site. In addition, docking results showed a lower binding energy for **3** (mixed type inhibition (-9.06 Kcal/mol); allosteric inhibition mode (-9.57 Kcal/mol)) than **2** (-7.51 Kcal/mol) and **1** (-7.95 Kcal/mol) for allosteric inhibition, which supports greater affinity of compound **3** and its greater binding capacity to the allosteric site. Further, **3** bound to allosteric site had similar number of H-bonds as **1** and **2** (Table 2, Fig. 4 and Fig. 5). However, van der Waals interactions between **3** and interacting residues were almost twice that of the other derivatives, indicating the importance of van der Waals interactions in addition to H-bond in terms of strengthening the protein-ligand complex, and suggesting this might be the reason for its better activity than other derivatives for AChE. Previously, we reported that the activity of isovitexin is greater than its aglycone apigenin in terms of diabetic complication and anti-AD activity (Choi et al., 2014). Also, compound **3** was

found to have twice the radical scavenging activity of **4** (Choi et al., 1994).

In addition, rubrofusarin and its derivatives were tested for their BACE1 inhibitory effects. All compounds, except **5**, showed promising inhibitory activity with  $IC_{50}$  values ranging from 14.41 to 190.63  $\mu$ M. However, compound activities did not follow the pattern as observed for AChE. Instead, activities followed the order **4** > **3** > **1** > **2** > **6** > **5**. **4** showed most potent inhibitory activity against BACE1 ( $IC_{50}$  = 14.41  $\mu$ M) which was more potent than of quercetin (21.42  $\mu$ M; positive control). Analysis of SARs indicated that the introduction of methoxyl group at C-8 position of **4** ( $IC_{50}$  = 86.05  $\mu$ M) in **2** ( $IC_{50}$  = 148.08  $\mu$ M) greatly decrease inhibitory activity, signifying the presence of hydroxyl group at C-8 position, like that observed for AChE activity, was essential for BACE1 inhibitory activity. In addition, comparing **5** (> 200  $\mu$ M) and **3** (85.66  $\mu$ M) against BACE1, revealed that the normal orientation (pyrone ring at  $\gamma$ -position of naphthalene ring) is essential for the BACE1 inhibitory activity whereas  $\beta$ -position attachment of pyrone ring resulted in a decrease or loss in activity.

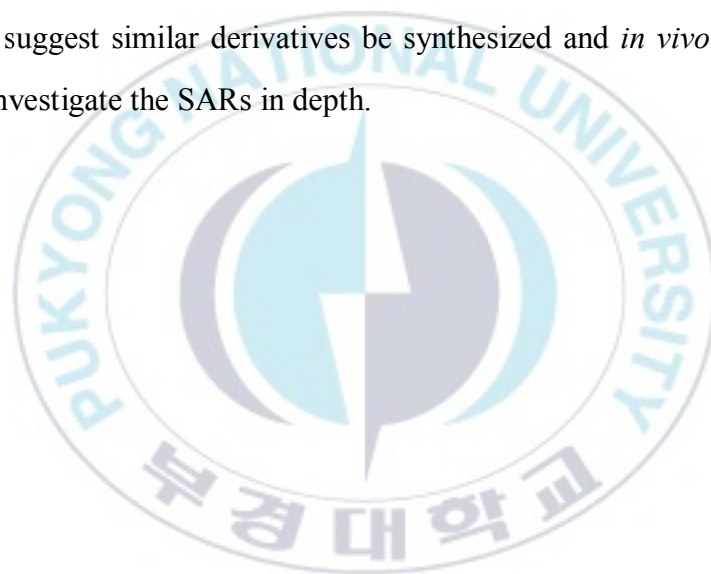
Further, kinetic and docking studies of **4** showed mixed type of inhibition whereas **2** demonstrated catalytic inhibition. QUD and PMF were used to simulate catalytic and allosteric site, respectively, as they are the reported selective inhibitors of BACE1. BACE1 has two main domains, that is, N-terminal domain and C-terminal domain with numerous detailed sub-regions distributed between them (Barman et al., 2013). The two aspartate residues, ASP32 and ASP228, in the cleft of the active site conserve the catalytic site of BACE1 (Hernández-Rodríguez et al., 2016) whereas SER10, THR 232, VAL336, and ALA157 compose the allosteric site of BACE1 (Youn et al., 2016). The BACE1-nor-rubrofusarin 6-*O*- $\beta$ -D-glucoside complex had a calculated binding energy -6.61 Kcal/mol attributed to six hydrogen bonds in the catalytic site, whereas in the allosteric site, six hydrogen bonds were formed with -8.34 Kcal/mol binding energy (Table 3). In contrast, **2** demonstrated competitive inhibition (binds to catalytic site of protein) and formed four H-bonds (lesser) and binding energy of -5.38 Kcal/mol (higher) compared to that of **4**. This implies the prominence of hydrophobic bonds, hydrogen bond distance and binding energy in addition to H-bond underlies the strength

of the protein-ligand interaction and the positioning of the inhibitor in the specific pocket.



## . Conclusion

The present study shows **3** and **4** inhibited AChE and BACE1 more potently than the other examined derivatives. Our result shows the presence of two glucose molecules, arrangement of pyrone at the  $\gamma$ -position of the naphthalene ring, and the substitution of methoxyl group with hydroxyl at C-8 on the naphthopyrone significantly enhance AChE inhibitory activity, whereas the presence of a single glucose, a pyrone ring at the  $\gamma$ -position of the naphthalene, and presence of hydroxyl group at C-8 of the naphthopyrone ring are essential for BACE1 inhibitory activity. From this study SARs of rubrofusarin and its derivatives isolated from *C. obtusifolia* were evaluated. Moreover, we suggest similar derivatives be synthesized and *in vivo* experiments be conducted to investigate the SARs in depth.



## . References

- Ali MY, Jannat S, Jung HA, Choi RJ, Roy A, Choi JS. Anti-Alzheimer's disease potential of coumarins from *Angelica decursiva* and *Artemisia capillaris* and structure-activity analysis. *Asian Pac J Trop Med*. 2016;9:103-111.
- Alzheimer's Disease International. World Alzheimer Report 2015: The global impact of dementia.
- Barman A, Prabhakar R. Elucidating the catalytic mechanism of  $\beta$ -secretase (BACE1): a quantum mechanics/molecular mechanics (QM/MM) approach. *J Mol Graph Model*. 2013;40:1-9.
- Cerella C, Teiten MH, Radogna F, Dicato M, Diederich M. From nature to bedside: Pro-survival and cell death mechanisms as therapeutic targets in cancer treatment. *Biotechnol Adv*. 2014;32:1111-1122.
- Chertkow H. Diagnosis and treatment of dementia: introduction. Introducing a series based on the third Canadian consensus conference on the diagnosis and treatment of dementia. *CMAJ*. 2008;178:316-321.
- Choi JS, Islam MN, Ali MY, Kim EJ, Kim YM, Jung HA. Effects of C-glycosylation on anti-diabetic, anti-Alzheimer's disease and anti-inflammatory potential of apigenin. *Food Chem Toxicol*. 2014;64:27-33.
- Choi JS, Lee HJ, Kang SS. Alaternin, cassiaside and rubrofusarin gentiobioside, radical scavenging principles from the seeds of *Cassia tora* on 1,1-diphenyl-2-picrylhydrazyl (DPPH) radical. *Arch Pharm Res*. 1994;17:462-466.
- Choudhury R, Chowrimootoo G, Srail K, Debnam E, Rice-Evans CA. Interactions of the flavonoid naringenin in the gastrointestinal tract and the influence of glycosylation. *Biochem Biophys Res Commun*. 1999;265:410-415.

- Dixon M. The determination of enzyme inhibitor constants. *Biochem Pharmacol.* 1953;55:170.
- Drever BD, Anderson WG, Riedel G, Kim DH, Ryu JH, Choi DY, Platt B. The seed extract of *Cassia obtusifolia* offers neuroprotection to mouse hippocampal cultures. *J Pharmacol Sci.* 2008;107:380-392.
- El-Halawany AM, Chung MH, Nakamura N, Ma CM, Nishihara T, Hattori M. Estrogenic and anti-estrogenic activities of *Cassia tora* phenolic constituents. *Chem Pharm Bull.* 2007;55:1476-1482.
- Ellman GL, Courtney KD, Andres V Jr, Featherstone RM. A new and rapid colorimetric determination of acetylcholinesterase activity. *Biochem Pharmacol.* 1961;7:88-95.
- Francis PT, Palmer AM, Snape M, Wilcock GK. The cholinergic hypothesis of Alzheimer's disease: a review of progress. *J Neurol Neurosurg Psychiatry.* 1999;66:137-147.
- Francis PT, Palmer AM, Snape M, Wilcock GK. The cholinergic hypothesis of Alzheimer's disease: a review of progress. *J Neurol Neurosurg Psychiatry.* 1999;66:137-147.
- Fukuda I, Kaneko A, Nishiumi S, Kawase M, Nishikiori R, Fujitake N, Ashida H, Structure–activity relationships of anthraquinones on the suppression of DNA-binding activity of the aryl hydrocarbon receptor induced by 2,3,7,8-tetrachlorodibenzo-p-dioxin, *J Biosci Bioeng.* 2009;107:296-300.
- Gechev TS, Hille J, Woerdenbag HJ, Benina M, Mehterov N, Toneva V, Fernie AR, Mueller-Roeber B. Natural products from resurrection plants: Potential for medical applications. *Biotechnol Adv.* 2014;32:1091-1101.

- Georgiev MI. From plants to pharmacy shelf. *Biotechnol Adv.* 2014;32:1051-1052.
- Graham JG, Zhang H, Pendland SL, Santarsiero BD, Mesecar AD, Cabieses F, Farnsworth NR. Antimycobacterial naphthopyrones from *Senna oblique*. *J Nat Prod.* 2004;67:225-227.
- Guha R. On exploring structure–activity relationships. *Methods Mol Biol.* 2013;993:81-94.
- Hatano T, Uebayashi H, Ito H, Shiota S, Tsuchiya T, Yoshida T. Phenolic constituents of Cassia seeds and antibacterial effect of some naphthalenes and anthraquinones on methicillin-resistant *Staphylococcus aureus*. *Chem Pharm Bull.* 1999;47:1121-1127.
- Hernández-Rodríguez M, Correa-Basurto J, Gutiérrez A, Vitorica J, Rosales-Hernández MC. Asp32 and Asp228 determine the selective inhibition of BACE1 as shown by docking and molecular dynamics simulations. *Eur J Med Chem.* 2016;124:1142-1154.
- Inestrosa NC, Alvarez A, Perez CA, Moreno RD, Vicente M, Linker C, Casanueva OI, Soto C, Garrido J. Acetylcholinesterase accelerates assembly of amyloid- $\beta$ -peptides into Alzheimer's fibrils: possible role of the peripheral site of the enzyme. *Neuron.* 1996;16:881-891.
- Jang DS, Lee GY, Kim YS, Lee YM, Kim CS, Yoo JL, Kim JS. Anthraquinones from the seeds of *Cassia tora* with inhibitory activity on protein glycation and aldose reductase. *Biol Pharm Bull.* 2007;30:2207-2210.
- Ju MS, Kim HG, Choi JG, Ryu JH, Hur J, Kim YJ, Oh MS. Cassiae semen, a seed of *Cassia obtusifolia*, has neuroprotective effects in Parkinson's disease models. *Food Chem Toxicol.* 2010;48:2037-2044.

- Jung HA, Ali MY, Choi JS. Promising inhibitory effects of anthraquinones, naphthopyrone, and naphthalene glycosides from *Cassia obtusifolia* on  $\alpha$ -glucosidase and human protein tyrosine phosphatases 1B. *Molecules*. 2016b;22:E28.
- Jung HA, Ali MY, Jung HJ, Jeong HO, Chung HY, Choi JS. Inhibitory activities of major anthraquinones and other constituents from *Cassia obtusifolia* against  $\beta$ -secretase and cholinesterases. *J Ethnopharmacol*. 2016a;191:152-160.
- Kim DH, Yoon BH, Kim YW, Lee S, Shin BY, Jung JW, Kim HJ, Lee YS, Choi JS, Kim SY, Lee KT, Ryu JH. The seed extract of *Cassia obtusifolia* ameliorates learning and memory impairments induced by scopolamine or transient cerebral hypoperfusion in mice. *J Pharmacol Sci*. 2007;105:82-93.
- Kitanaka S, Takido M. Studies on the constituents in the roots of *Cassia obtusifolia* L. and the antimicrobial activities of constituents of the roots and the seeds. *Yakugaku Zasshi J Pharm Soc Jpn*. 1986;106:302-306.
- Kryger G, Silman I, Sussman JL. Structure of acetylcholinesterase complexed with E2020 (Aricept): implications for the design of new anti-Alzheimer drugs. *Structure*. 1999;7:297-307.
- Lee GY, Jang DS, Lee YM, Kim JM, Kim JS. Naphthopyrone glucosides from the seeds of *Cassia tora* with inhibitory activity on advanced glycation end products (AGEs) formation. *Arch Pharm Res*. 2006;29:587-590.
- Lee HJ, Jung JH, Kang SS, Choi JS. A rubrofusarin gentiobioside isomer from roasted *Cassia tora*. *Arch Pharm Res*. 1997;20:513-51.
- Lim SS, Jung YJ, Hyun SK, Lee YS, Choi JS. Rat lens aldose reductase inhibitory constituents of *Nelumbo nucifera* stamens. *Phytother Res*. 2006;20:825-830.

- Lineweaver H, Burk D. The determination of enzyme dissociation constants. *J Am Chem Soc.* 1934;56:658-666.
- Luo J, Hu Y, Kong W, Yang M. Evaluation and structure-activity relationship analysis of a new series of aryl naphthalene lignans as potential anti-tumor agents. *PLoS One.* 2014;9:e93516.
- Ma DL, Chan DSH, Leung CH. Molecular docking for virtual screening of natural product databases. *Chem Sci.* 2011;2:1656-1665.
- McKinney JD, Richard A, Waller C, Newman MC, Gerberick F. The practice of structure-activity relationships (SAR) in toxicology. *Toxicol Sci.* 2000;56:8-17
- Megawati, Dewi RT, Mulyani H, Maryani F, Lotullung PND, Minarti. Rubrofusarin from *Aspergillus niger* GTS01-4 and its biological activity. *AIP Conf Proc.* 2017;1803:020026.
- Meng XY, Zhang HX, Mezei M, Cui M. Molecular docking: a powerful approach for structure-based drug discovery. *Curr Comput Aided Drug Des.* 2011;7:146-157.
- Messana I, Ferrari F, Cavalcanti MS, Morace G. An anthraquinone and three naphthopyrone derivatives from *Cassia pudibunda*. *Phytochemistry.* 1991;30:708-710.
- Metwally K, Khalil A, Sallam A, Pratsinis H, Kletsas D, El SK. Structure-activity relationship investigation of methoxy substitution on anticancer pyrimido[4,5-c]quinolin-1(2H)-ones. *Med Chem Res.* 2013;22:4481-4491.
- Morris GM, Lim-Wilby M. Molecular docking. *Methods Mol Biol.* 2008;443:365-382.
- Na M, Jin WY, Min BS, Ahn JS, Bae KH. Protein tyrosine phosphatase 1B inhibitory activity of anthraquinones and stilbenes. *Nat Prod Sci.* 2008;14:143-146.

- Park TH, Kim DH, Kim CH, Jung HA, Choi JS, Lee JW, Chung HY. Peroxynitrite scavenging mode of alaternin isolated from *Cassia tora*. *J Pharm Pharmacol*. 2004;56:1315-1321.
- Ratty AK, Das NP. Effects of flavonoids on nonenzymatic lipid peroxidation: structure-activity relationship. *Biochem Med Metab Biol*. 1988;39:69-79.
- Sato H, Chuang VT, Yamasaki K, Yamaotsu N, Watanabe H, Nagumo K, Anraku M, Kadowaki D, Ishima Y, Hirono S, Otagiri M, Maruyama T. Differential effects of methoxy group on the interaction of curcuminoids with two major ligand binding sites of human serum albumin. *PLoS One*. 2014;9:e87919.
- Schnekenburger M, Dicato M, Diederich M. Plant-derived epigenetic modulators for cancer treatment and prevention. *Biotechnol Adv*. 2014;32:1123-1132.
- Schultz TW, Dumont JN, Sankey FD, Schmoyer RL. Structure activity relationships of selected naphthalene derivatives. *Ecotoxicol Environl Saf*. 1983;7:191-203.
- Schulz V. Ginkgo extract or cholinesterase inhibitors in patients with dementia: what clinical trials and guidelines fail to consider. *Phytomedicine*. 2003;10:74-79.
- Tricco AC, Soobiah C, Lillie E, Perrier L, Chen MH, Hemmelgarn B, Majumdar SR, Straus SE. Efficacy of cognitive enhancers for Alzheimer's disease: protocol for a systematic review and network meta-analysis. *Syst Rev*. 2012;1:31.
- Vassar R. BACE1: the beta-secretase enzyme in Alzheimer's disease. *J Mol Neurosci*. 2004;23:105-114.
- Weymouth-Wilson AC. The role of carbohydrates in biologically active natural products. *Nat Prod Rep*. 1997;14:99-110.
- Wong SM, Wong MM, Seligmann O, Wagner H. New antihepatotoxic naphtho-pyrone glycosides from the seeds of *Cassia tora*. *Planta Med*. 1989;55:276-280.

- Yanagita RC, Kamachi H, Kikumori M, Tokuda H, Suzuki N, Suenaga K, Nagai H, Irie K. Effects of the methoxy group in the side chain of debromoaplysiatoxin on its tumor-promoting and anti-proliferative activities. *Bioorg Med Chem Lett*. 2013;23:4319-4323.
- Yen GC, Chuang DY. Antioxidant properties of water extracts from *Cassia tora* L. in relation to the degree of roasting. *J Agric Food Chem*. 2010;48:2760-2765.
- Yi JH, Park HJ, Lee S, Jung JW, Kim BC, Lee YC, Ryu JH, Kim DH. *Cassia obtusifolia* seed ameliorates amyloid  $\beta$ -induced synaptic dysfunction through anti-inflammatory and Akt/GSK-3 $\beta$  pathways. *J Ethnopharmacol*. 2016;178:50-57.
- Youn IS, Han AR, Choi JS, Seo EK. A New Naphthalenic Lactone Glycoside from the Seeds of *Cassia obtusifolia*. *Chem Nat Compd*. 2017;53:1-3.
- Youn K, Lee J, Ho CT, Jun M. Discovery of polymethoxyflavones from black ginger (*Kaempferia parviflora*) as potential  $\beta$ -secretase (BACE1) inhibitors. *J Funct Foods*. 2016;20:567-574.
- Zhang C, Wang R, Liu B, Tu G. Structure elucidation of a sodium saltified anthraquinone from the seeds of *Cassia obtusifolia* by NMR technique assisted with acid-alkali titration. *Magn Reson Chem*. 2011;49:529-532.